Short-term Glacial Calving Processes at Kronebreen-Kongsvegen, Svalbard

A Thesis

Submitted for consideration to the

Department of Geology

at

Bryn Mawr College

By Phaedra Calista Tinder

in partial fulfillment of the Bachelor of Arts degree,
May, 2010

Thesis Advisor: Donald C. Barber

ABSTRACT

Calving is an important component of glacier mass loss, but it remains difficult to model and directly influences sedimentological processes at the ice margin. As part of the Svalbard REU, this study aims to characterize the short-term calving processes at a tidewater glacier and establish a baseline dataset to which future and contemporary studies can be compared. The study was conducted during two weeks in July and August of 2009 at the head of Kronebreen-Kongsvegen glacier system in Kongsfjorden, Svalbard. Two water pressure gauges deployed on the north and south sides of the fjord, adjacent to the glacier face, logged water levels at ten-second intervals. Air pressure and fjord salinity were used to convert water pressure to water depth. The higher frequency water level changes were analyzed to identify large calving events and study their frequency, size, and origin along the calving front. The timing and magnitude of calving events also were compared with potential external forcing mechanisms, such as weather, tidal stage, and local water depth. The pressure-logged wave records were calibrated and confirmed by comparison with observational data from visual logging of calving events at the site.

The 15-day study period occurred during the height of the summer melt season. Over the entire record, the frequency of calving events appears to follow the changing tidal amplitude, with reduced calving after the neap tide interval. The observed relationship between calving frequency and tidal stage has been documented at Alaskan glaciers and other locations, and linked causatively by the explanation of increased circulation at the glacier front, as well as the destabilizing effect of buoyancy on the ice front. Fjord water depth at the glacier front influences the formation of “calving bays” where a majority of calving events were observed and the majority of ice loss occurred, as confirmed by satellite imagery.

This project is part of a multi-year study of the response of Kronebreen-Kongsvegen to climate change, and also addresses the problem of constraining calving mechanisms and dynamics. Proper methodology in association with deployment of multiple water depth/pressure loggers placed close to a calving glacier terminus are recommended as an effective means of studying calving processes at a high resolution over various time intervals.

DEDICATION

This thesis is dedicated to Mr. Hansen, Ms. Cioffi, Mrs. Kaelin, Mrs. Miller, Ms. Pawlowski, and Dr. Richardson, science teachers from elementary to high school, without whose inspiration I might have been a Literature major.

Also to Mrs. Maddox, Mr. McConkey, Ms. Probst, Rachel Carson, Susan Jeffers, Dr. Seuss, Really Wild Animals, my parents, and the Environmental Learning Center in Vero Beach, Florida, who early on taught me the value and importance of environmental conservation.

"When the climbers in 1953 planted their flags on the highest mountain, they set them in snow over the skeletons of creatures that had lived in the warm clear ocean that India, moving north, blanked out. Possibly as much as twenty thousand feet below the seafloor, the skeletal remains had turned into rock. This one fact is a treatise in itself on the movements of the surface of the earth. If by some fiat I had to restrict all this writing to one sentence, this is the one I would choose: The summit of Mt. Everest is marine limestone."

-*John McPhee,* Basin and Range

"When we try to pick out anything by itself, we find it hitched to everything else in the universe."

-*John Muir,* My First Summer in the Sierra

“If your knees aren't green by the end of the day, you ought to seriously re-examine your life.”

-*Bill Watterson,* Calvin and Hobbes

ACKNOWLEDGEMENTS

This project was graciously supported by the National Science Foundation's Research Experiences for Undergraduates program (grant 0640096). Thanks to Bryn Mawr College's Watson Fund for support of institutional elements of the study as well as transportation to the Arctic Workshop. Norsk Polar Institut and University Centre on Svalbard provided invaluable logistical and technical support and advice while in Svalbard, deserving much thanks. Especially strong thanks to Wojtek Moskal at NPI, who was tireless in his support and assistance.

I would like to especially thank my advisors, who inspired a depth of study and investigation to allow the production of this project: Professor Arlo Weil, whose instruction in the Senior Thesis seminar provided excellent resources for the production of the written thesis; Professor Don Barber, who provided invaluable advice, insight, and support for the analyses of the project undertaken at Bryn Mawr; and Professors Julie Brigham-Grette and Ross Powell, who taught the REU students much while in Svalbard and were crucial to the development and understanding of the field work and analysis being undertaken. Additionally, all of the TUSKer students -- Laura K., Laura P., Theo, Hector, and Hannah -- and the co-PI's of the Svalbard REU, Steve Roof and Al Werner, who all made this a memorable academic and personal experience. Finally, fellow BMC geology seniors – Tanya, Sophia, Anne, Maryann, Michelle, and Nithya – as well as all the geology students who have been friends and supporters while I've been at Bryn Mawr.

TABLE OF CONTENTS

LIST OF FIGURES

LIST OF TABLES

INTRODUCTION

Glacier mass balance modeling has become an important area of research in recent years in light of global concerns about climate change and sea level rise. Arctic ice masses (except Greenland) account for a relatively small proportion of the global ice on land, but because temperatures in the Arctic are typically higher than in the Antarctic, Arctic ice is likely to melt more rapidly and thus will have a greater influence on sea level change in the near future (Dowdeswell et al., 1997; Meier et al., 2007). Several recent studies have shown strong evidence that glaciers are responding to climate changes more rapidly than previously expected (Hagen et al., 2005, Bamber et al., 2007, Howat et al., 2008). In this context, it is important to understand the mechanisms controlling the various elements that play into glacier mass balance, and how external factors control the magnitudes of changes in that balance.

Glacier mass balance consists of both ice loss and ice gain. Ice gain occurs through surface accumulation (e.g., snowfall), and typically is highest during the winter (Hagen et al., 2003). Ice loss occurs through surface melting, calving (iceberg production), and bottom melting of floating ice (Oerlemans and Nick, 2006). Surface melting on Svalbard is largely a function of altitude, which is mostly reflective of air temperature, and no floating ice shelves have been observed on Svalbard (Hagen et al., 2003). In general, ice flux at calving margins is estimated from observations of glacier velocity, thickness, and horizontal width at the terminus (Hagen et al., 1999).

Calving represents the largest proportion of mass loss for most tidewater glaciers (glaciers terminating in the ocean that are grounded, without a floating shelf), yet is still difficult to model and poorly understood (Amundson et al., 2008). Considerable research effort continues to focus on both field and theoretical techniques that might better constrain predictions and may facilitate monitoring of changes occurring in glaciers and ice sheets. This study focuses solely on monitoring the process of calving as a component of mass loss.

Glaciers are broadly defined by climate zone as polar, subpolar, and temperate. This glacier classification reflects, among other things, the coupling between the glacier bottom and

the subglacial till: where basal ice is frozen to the underlying substrate, it is called cold-based; if basal meltwater or rock surface, it is wet-based; glaciers with basal conditions between these end members are referred to as polythermal. The amount of meltwater at the subglacial surface is one of the most important controls on glacial sliding velocity, as it decreases basal friction. Glaciers that are cold-based for the entire year experience movement only through internal ice deformation, because basal sliding does not occur (Benn and Evans, 1998). Svalbard's glaciers have been broadly described as polythermal (Blasczyck et al., 2009), but characterizing them more precisely is a key interest of the multi-year Svalbard REU of which this project was part.

Studies have focused on both the internal and external components affecting calving rates and dynamics (Benn et al., 2007). Mechanically, a calving event is produced when a crevasse (a fracture in the surface of the glacier) moves, by glacial flow and calving at the ice front, to the tidewater front and the fracture propagates fully, separating the calved ice mass from the remainder of the glacier (Pralong and Funk, 2005; Weiss, 2004). Alley et al. (2008) proposed a calving law that accounts for the physical, or internal, basis of iceberg calving. The model by Alley and others (2008),

$$c = 15{,}000 e^{-0.43} \qquad [1]$$

where c is the calving rate and e is the spreading rate of the glacier ice front parallel to the front, accounts for 80-90% of the variance in calving rate (Alley et al., 2008). Previous studies have focused on the internal forces producing calving by investigating the factors that contribute to crevasse formation and propagation, including stretching associated with the gradient of the flow; research has also targeted the forces acting on the glacial tongue, such as buoyant and undercutting forces as a result of interaction with the body of water (Benn et al., 2007).

External factors that influence calving are those environmental conditions that produce or influence the magnitude of the internal mechanisms. Previous studies have studied the effects of environmental variables and found tidal fluctuations and water depth at the front of the glacier to be significant factors (Brown et al., 1982; O'Neel et al., 2003). Substantial evidence also

indicates a statistically significant difference in calving rates between freshwater- and saltwater-terminating glaciers (with the latter being higher), but whether this is caused by a lower melting point produced by higher salinities or differences in circulation patterns of the water at the front of the glacier remains undetermined (Benn et al., 2007). Many previous studies have utilized seismology and subjective observation to monitor calving events (Qamar, 1988, O'Neel et al., 2007; Brown et al., 1982). However, given the demand for increased monitoring of glacier change, cost-effective methods and remotely deployed monitoring techniques need to be examined in order to gather higher quality data more efficiently.

Increased monitoring is important for determining how different types of glaciers respond to various forcings. Temperate tidewater glaciers in Alaska (e.g., Columbia, Mendenhall, LeConte) have been extensively monitored and studied with regard to calving, but there have been fewer calving studies at other marine margins. In the Alaskan studies, basal sliding velocity of the glacier has been closely tied to calving rate (Brown et al., 1982; Benn et al., 2007). Regional climate is an important factor in controlling the production of basal meltwater, which decreases friction on the glacier bed and can produce basal sliding. Therefore, it is likely that tidewater glaciers from different temperature regimes respond differently to climate change, and as a result, may have different patterns of mass loss due to iceberg calving.

This paper analyzes water depth/pressure logger data collected near the calving margin during the summer melt season of July-August 2009 at Kronebreen-Kongsvegen, Western Spitsbergen, Svalbard. In doing so, the potential for using water level sensors for monitoring calving events at this site is assessed. The resulting observational data are analyzed to test for connections among the potential external forcing mechanisms (tidal fluctuations and weather) and the frequency and magnitude of calving events. The mechanisms that produce calving events are complex; thus it is unsurprising that no strong correlations are observed for any individual factor. However, the study provides baseline calving data and serves as a "proof of concept" for future monitoring efforts.

SITE BACKGROUND: KONGSFJORDEN AND KRONEBREEN/KONGSVEGEN

Kongsfjorden is an estuarine fjord located in northwest Spitsbergen, which is the western island of Svalbard, an archipelago in the Norwegian High Arctic (see Figure 1). Kronebreen and Kongsvegen are two converging tidewater glaciers located at the southernmost end of Kongsfjorden at 79°N 12.5°E (Svendsen et al., 2002). Kronebreen covers the majority of this front and is actively calving, while Kongsvegen has mostly retreated out of the water and calves infrequently. The combined ice front of Kronebreen and Kongsvegen is approximately 3.5km wide, and includes two "calving bays" in which calving is typically more frequent during the melt season (Trusel et al., in press). The terminal margins of both glaciers have retreated substantially in the past decade (Kaab et al., 2005; Trusel et al., in press).

On the southern side of the fjord is an ice-marginal delta that formed during the past decade (Trusel et al., in press). The bathymetry of the southern side of the fjord is much shallower (averaging about 30m) while water depths on the northern side and in the center of the fjord range from 50 to more than 80 m (Trusel et al., in press; Kehrl et al., 2010). There are two localized areas of high meltwater discharge high in sediment, one from the delta area, and the other from the northern side. During the study period, a separate study monitored sediment discharge in order to evaluate connections between iceberg calving and other mechanisms of sediment transport; the results of those monitoring efforts are reported elsewhere (Barnhart et al., 2010; Kehrl et al., 2010; Marshburn et al., 2010; Poppick et al., 2010; Zamora et al., 2010).

Kongsfjorden is under frequent monitoring because of its proximity to Ny Ålesund, the world's northernmost permanent settlement and a high-tech Arctic research village. The potential for cross-comparison of glacial monitoring data with a variety of other biological, geophysical, and oceanographic studies in close proximity to one another provides a compelling context for the results presented here.

METHODS

I. Field Methods

Field data were collected in Kongsfjorden, NW Spitsbergen, Svalbard, at 79°N/12.5°E, from July 28, 2009 to August 12, 2009. HOBO® U20-001-01-Ti 30-Foot Depth Titanium water depth/pressure loggers were placed at two locations adjacent to the front of the Kronebreen-Kongsvegen glaciers in Kongsfjorden at stations on opposite sides of the glacier face judged to be suitably protected from icebergs. The gauges were programmed to record every 10 seconds (allowing for continuous logging for about 2.5 days between data downloads). Three other data sets with higher temporal resolution were also logged: one with a 1-second recording interval and two that logged every 5 seconds. These higher frequency records were used for quality control comparisons. Data from the pressure loggers were off-loaded and the instruments were re-deployed at stations on the northern ("Rock") and southern ("Delta") sides of fjord on alternating days. GPS locations were recorded at each re-deployment to ensure consistency. The pressure-loggers were mounted inside a 0.3m-long PVC tube and attached with rope to a 15-kg rock to prevent lateral movement. The weight and tube were attached to a rope that was anchored above water at the site for ease of retrieval and to prevent instrument loss.

Throughout the study, a record of visually observed calving events was kept. For every observed calving event, the time, approximate visual size, and source location were recorded. The ice front was divided into five roughly equal-sized zones based on structural features (illustrated in Figure 1), and the position of calving events within these zones was recorded. The observational record is both subjective and incomplete, due to observational biases resulting from the location of the boats throughout the day and a need to complete other field tasks that sometimes precluded recording calving events, especially smaller ones.

Other data were collected concurrently as a part of this and continuing studies of the Kongsfjorden glacial system. Conductivity, Temperature, and Depth (CTD) and Optical Back-Scatter (OBS) scans were done using a Seabird SBE 19*plus* V2 SEACAT Profiler in daily

transects out from the two sediment sources at the glacier front. Sediment traps were deployed and gravity cores were collected along these same transects to examine current and past sedimentation rates. Rock and ice samples were collected from various sources within the fjord to study sedimentary provenance. Bathymetry surveys were conducted using an echosounder and compared with data collected in 2005 to assess sedimentation rates and dispersion (Trusel et al., in press). The analysis and interpretation of these data are reported elsewhere in the reports by the other students of the 2009 REU project.

II. Data Analysis

Water depth/pressure logger data processing

The raw water depth/pressure logger data required filtering and correction for tidal variations and other, more abrupt artifact elements in the records. The raw data (converted from water pressure to depth using the Hoboware Pro software) are shown in Figure 2 and the adjusted data, post-correction, are shown in Figure 3. Diurnal variations in water level due to the lunar tides were removed by subtracting a linearly interpolated hourly water depth/pressure logger record reported by the Norwegian Meteorological Institute (online vannstand.statkart.no). Large, near-instantaneous frame-shifts also occurred in the raw record, apparently due to abrupt vertical movements of the water depth/pressure logger along the fjord floor into deeper or shallower water. Problematically, these shifts were often caused by waves associated with large calving events, which made accurate determination of true calving wave amplitude difficult. The frame-shifts were manually corrected by marking separate intervals for subtraction of the Ny Ålesund tide records. To more accurately assess wave amplitudes, an additional correction method and filtering system was applied, after all of the calving events had been identified.

Identification of calving events

After correcting for tidal oscillations, the remaining record represents water level deviations from a flat water surface. To distinguish water level fluctuations (waves) caused by calving events from those caused by wind, seiches, or other water disturbances (e.g., boat wakes), the water level records were assigned statistical z-score values,

$$\left|\frac{X_t - \mu_x}{\sigma_x}\right| > 1 \qquad [2]$$

where X_t is the water level at time *t*, μ_x is the mean water level (in this case, μ_x=0, or flat water), and σ_x is the standard deviation of the water level record. Records with a z-score less than one standard deviation from the mean were excluded. Filtered data were then manually examined to identify calving event waves. The selected calving events had a substantially higher frequency than the mostly flat background, and were coded by an acceptable z-score. For each identified event, the initial arrival time, maximum waterlevel, minimum waterlevel, and duration of the event were recorded. The difference between the maximum and minimum water level over the duration of the event was called the "wave amplitude." To correct discrepancies caused by the previous frame-shift adjustment, it was sometimes necessary to further adjust the amplitude measures. Differences between maximum and minimum amplitude values for a given event were compared, and if greater than 0.01 (the decimal resolution of the data), their values were corrected to a mean of 0 and their amplitude adjusted by subtracting half the amplitude difference. Finally, the amplitude:duration (time to attenuation) ratio of individual wave events was used to filter out events characterized by unrealistically long durations.

Localization and Calibration of Calving Events

Transects were drawn on the bathymetry map (Kehrl, 2010) between each water depth/pressure logger mooring and the boundaries of the calving zones on the glacier front (see Figure 4). The basemap utilizes a georeferenced ASTER image at 15m resolution taken on August 1, 2009, during the present study period. The distance and average depth along these transects were determined (see Table 1 and 2), and used to calculate wave velocity within the fjord:

$$\text{Shallow water wave:} \quad v = \sqrt{gh} \qquad [3]$$

$$\text{Transitional Deep- to Shallow-water wave:} \quad v = \sqrt{\frac{gh}{2\pi} * \tanh\left(\frac{2\pi\lambda}{h}\right)} \qquad [4]$$

$$\text{Deep water wave:} \quad v = \sqrt{\frac{g\lambda}{2\pi}} \qquad [5]$$

where v is the velocity of the wave, g is the gravitational constant (g=9.81 m/s^2), h is the water depth, and λ is the wavelength. Summaries of these calculations are reported in Table 3. These estimates were used to identify pairings between visual observations of calving events and the subsequent recording of elevated water levels by the water depth/pressure logger at one or both tide gauge stations.

Next, the difference in estimated surface wave travel time was calculated for each zone boundary to provide boundaries for localization estimates (see Figure 5 and Table 4). The differential arrival times at each station theoretically provide a unique source for waves of similar wavelengths (see Figure 6a). These travel-time estimates were additionally compared with the visually observed events whose signals were recorded at both stations (see Table 4).

Finally, these estimates were applied to a randomly selected sample of recorded calving events that had an interpreted corresponding event recorded at both the Delta and Rock stations. Events were identified as corresponding if the initial wave arrival times at the opposite tide gauges were within four minutes of each other, which is a standard based on the calculated

expected wave travel times (see Table 4). Using the boundary limitations, the approximate source of each event was estimated for each model and compared with the visually observed events data. Then the approximate size of the original wave amplitude was estimated, using the assumption (from Ward, 2001) that wave amplitudes attenuate according to the function

$$a_{received} = \frac{a_{source}}{\sqrt{r}} \quad [6]$$

where $a_{received}$ is the maximum adjusted amplitude recorded at water depth/pressure logger, a_{source} is the original amplitude formed by the calving iceberg at the glacier front, and r is the length of the transect that the wave travelled between the source and the water depth/pressure logger station. This idealized attenuation pattern is consistent with the observed relationship between the distance travelled by a calving wave and the observed wave amplitude recorded at the logger station, for paired events with a visually observed subjective iceberg size (see Figure 6b).

RESULTS

I. Time series analysis

Time-series analysis was done to assess relationships between calving rates and various measured external factors. The considered external factors are tidal variation, air temperature variability, and precipitation time, all measured at the Ny Ålesund meteorological facility (see Figure 7). The logged calving data were re-sampled to calculate daily, quarter-day (six-hour), and hourly calving rates for both stations (see Figures 8, 9). As a closer estimate of ice mass loss, the maximum, average, and summed adjusted wave amplitudes were calculated over daily, quarter-daily, and hourly timescales for the wave patterns recorded at each mooring station (see Figures 10-12).

The average wave amplitude at the Rock mooring station is substantially larger than at the Delta station overall. Because brash ice tended to build up on the south side of the fjord, waves traveling to the Delta mooring station may have been damped by the floating mass of ice. The shoreline bathymetry was also different on each side, with the Delta having a shallower, beach-like underwater slope while the Rock had steeper slopes both underwater and above-water. Both of these factors could produce differences in recorded wave amplitude. However, if the majority of calving events occurred on the north side of the ice front (proximal to the Rock station), then the incident waves would be expected to be larger at the Rock station regardless of the site bathymetry or damping by brash ice. The degree to which the recorded wave size is directly indicative of calving size as opposed to an artifact of the site bathymetry is important to consider in the second phase of analysis.

In assessing the degree to which external factors are related to the pattern of calving events, various weak correlations are noted between the environmental variables and calving events (see Table 5). There are weak correlations between air temperature and several measures of calving at both the Delta and Rock stations, as well as between precipitation and calving. Diurnal high tide height is notably not correlated with any measure of calving, except for a weak correlation (r=0.21) with the average calving wave amplitude at the Delta station. When considering a lag time, however, various calving measures correlate with the daily high tide level to a higher degree than either precipitation time or air temperature without lag (see Table 6). Previous studies (e.g., Benn et al., 2007, Brown et al., 1983, O'Neel et al., 2003, Van der Veen, 2002) have reported a proportional relationship between higher tide elevations and higher calving rates, and the data here support this conclusion. At the Delta station, the correlation is strongest with lag times of 2, 6, and 7 days (r=0.58, 0.56, and 0.72, respectively), and at the Rock station, the correlation is strongest with a 2 day lag (r=0.51).

An additional question is whether calving measures varied by daily tidal phases (high tide, low tide, rising tide, falling tide) (see Figures 13-16). Some differences are apparent, such as a mean higher wave amplitude at high and low tides and lower wave amplitude during rising and falling tide, received at the Delta station. In spite of this observation, single-variable ANOVA

analyses show no significant variations in calving rates with respect to tidal phase (high, low, rising, falling) (see Tables 7-10). Nevertheless, an oscillatory pattern lagging high tide by approximately 3 days can be seen in the calving rates per tidal phase at the Delta station, although no such pattern is apparent in the Rock record (see Figure 17).

II. Calving localization

The calving event data were analyzed spatially in order to gain information that could be extrapolated to the larger dataset. The visually observed events that were paired with signals received by one or both of the pressure logger stations ("paired events") are shown in Figure 18. Because of the subjective nature of the visual data, these estimations of iceberg size were compared with the recorded wave amplitude received at the logger stations (Figure 19). Localizing these wave signals allowed for the creation of ratings curves, showing the relationship between the amplitude of the wave signal at the logger and the travel time (Figures 20, 21) and the relationship between the amplitude of the wave signal received at each station, for paired events recorded by both stations (Figure 22). Travel time was calculated by the difference between the time the event was visually observed and the initial reception of the anomalous wave signal at the pressure logger. These curves had mixed levels of significance (see Tables 11 and 12 for the linear regressions produced for each station). This analysis also allowed for an understanding of the range of amplitudes per zone for paired events (Figures 23, 24). At the Delta station, the largest wave amplitudes tended to originate closest to the station, with Zone 4 and Zone 4-5 sourcing the largest-amplitude waves. At the Rock station, the highest mean wave amplitude also originated from Zone 4-5, indicating that this zone probably produced the largest iceberg events. However, the overall trend that events in closer proximity to the pressure logger station tended to be received as larger wave signals persists. The range of paired event sizes by subjective observation is shown in Figure 25, which concurs with the amplitude data on the tendency for large events in Zone 4, and also shows a high average event size from Zone 1-2.

This information was applied to the larger dataset by estimating sources for events recorded by both logger stations but not visually observed. These inferred calving events are termed “penecontemporaneous events” or “PEs”. Calving localizations were inverted for 98 randomly selected events (out of a total of 408 PEs) by using the difference in arrival times at the two stations (Table 13). The localizations are shown for each of the three wave travel models (Eqs. 3-5) as well as the estimates gained from the analysis of paired events (see Table 4). The resolution of these interpretations is at the scale of the zone boundaries. These data are also compared with the proportion of visually observed events originating in each zone region (Table 14). While the proportion of events occurring in each zone varies substantially based on the boundary conditions used, most of the frameworks identify Zone 1-2 and either Zone 3-4 or Zone 4-5 as the sources for the majority of events. The visually observed events have a fairly even distribution of events at Zone 1-2, 2-3, 3-4, and 4-5 although there was spatial heterogeneity in the size of the visually observed events.

The source analyses were used to estimate initial calving amplitudes of the PEs, using the distance to that endpoint as the distance the wave traveled, allowing for rough estimation of its attenuation by using equation 6. The range of wave amplitudes from each zone source for each of the boundary models is shown in Figure 26. The models show a similar trend as that observed in the paired events data, with the largest events occurring around Zone 4 with a secondary peak in event size around Zone 2.

DISCUSSION

I. Comparison of calving event descriptions

In this study, calving events have been described by a number of different standards. One issue is reconciling the subjective observations of iceberg size with the resulting wave amplitude signals received at the water level monitoring stations. These two measures are

positively correlated in paired events, and the correlation is stronger when only events close to the station are included (i.e., events for which a large event would not be far enough away to suffer substantial wave attenuation) (Figure 19). This indicates that both methods (visually observed and pressure logging) are reasonably reliable measures of calving size, despite acknowledged uncertainties. For instance, the visually observed subjective calving size is a representation of the size of the iceberg produced by the calving event, and thus the approximate volume of water being moved to create the waves received at the pressure logger stations. However, the visual method is uncertain in that, of necessity, it discretely represents a continuous value (that of iceberg volume), in addition to being subject to all the pitfalls of a human-based subjective assessment. Furthermore, the simplification of the visual observations into indexed discrete size values, does not take into consideration other meaningful elements of the calving event, for instance whether it occurs in portions or instantaneously and whether it falls from high on the glacier front or emerges from below the water. These elements add variability that will complicate the relationship with the amplitude of the waves produced by the calving event.

An additional area of possible error is in the signal processing and conversion of the raw data, especially the amplitude adjustment made to correct for the shifting pressure logger along the fjord floor. The majority of these amplitude adjustments are coincident with vertical frame-shifts in the data. It is also important to consider whether the results are artificially biased by the sampling interval, which was predominantly at 10-second intervals. Comparisons of the 1-second, 5-second, and 10-second sampling intervals reveal that neither the number nor the amplitude of events recorded varies, although at shorter sampling intervals, events are easier to identify and the wave arrival time can be more precisely determined.

A final consideration in using wave amplitudes as a proxy for calving event size is the identification and selection of the proper wave segments, and how to represent that waveform numerically to compare it to other events. The identification process is rigorous, as described in the Methods section. The means for representing the wave amplitude data, however, are still varied. Whether to use the daily, hourly, or 6-hour rates, or the average, sum, or maximum values over these timescales is an important consideration because, as Figures 8-12 show, the

different approaches do not produce identical representations of the calving data. A single measure has not been used throughout this study, recognizing both that various relationships occur on different timescales and that different mechanisms are reflected in different representations. The correlations matrix in Table 5 illustrates that each measure is uniquely related to the environmental factors.

II. Roles of Environmental Variables

Air temperature and Precipitation Time

The three primary environmental (or external) variables that are considered are: precipitation duration, air temperature, and tidal height (see Figure 7). Multiple-regression models were calculated with the quarter-day calving rate as the dependent variable and each of these environmental variables as independent variables (Tables 15, 16). The 6-hour calving rate was selected because this is the time-sampling interval of the precipitation data obtained from the Norwegian Meteorological Institute; tidal height and air temperature are likewise averaged over these intervals. The models show very little significance in the relationships between precipitation or tidal height (without lag) with either the Delta or Rock station wave amplitude records (adjusted R^2<0.1 and P>>0.05). The only indication of a meaningful relationship indicated here is with air temperature at the Delta station; in this instance, the P-value for air temperature is P=0.06, quite close to the traditional cutoff level of P=0.05 for 95% confidence. While this is not enough to support a conclusive relationship, it indicates that future studies, perhaps on longer timescales, might observe a significant relationship between air temperature and calving rate. This would be expected since air temperature is generally considered a proxy for surface melting (Dowdeswell, pers. comm., 2010), and the larger pattern of freeze-and-melt has seasonal temperatures as its primary forcing. Nevertheless, the present data do not causatively show whether or not temperature changes have a marked influence on short-term calving processes.

The potential effect of precipitation events on calving events was examined graphically (Figures 8b, 9b). There are three identifiable precipitation events over the study period. Two precede periods when calving event frequency increased at the Delta and Rock stations, while one has no apparent effect. The result of a flood of freshwater on circulation at the glacier terminus, or simply the flooding and breakage of crevasses, causing calving, are two possible explanations for the effect of precipitation causing higher calving rates. These mechanisms are similar to the effect observed by O'Neel et al. (2003) at LeConte glacier in Alaska, with precipitation having a noticeable impact, but the exact relationship being difficult to elucidate.

The correlations matrix in Table 5 shows various weak linear relationships between air temperature and precipitation time with different calving measures. That the strongest relationships tend to be with measures of mass loss, as opposed to total events, no matter the size, indicates that precipitation and air temperature may have more influence on the occurrence of larger events and the total mass lost, as opposed to small breakage pieces, which may be a more stochastic process. This reflects the calving law produced by Alley et al. (2008) (Eq. [1]) in that larger events are more likely to be the result of forcings that can affect the overall ice flow and thus the glacier's spreading rate.

Tidal Oscillation

While the aforementioned analyses do not find any significant relationship between tidal fluctuations and calving rates, assessments that consider a lag time between the tidal wave and a corresponding change in calving find statistically significant relationships stronger than those observed with temperature or precipitation (Table 6). Multiple moderate-to-strong correlations are observed that suggest different possible lag times. The strongest correlations are with the Delta record with a lag time of 7 days, using the measures of the daily calving rate ($r=0.72$) and the summed daily calving event amplitudes ($r=0.85$). These measures are the two most related to the bulk number of events as opposed to the volume of ice being lost. It is puzzling, however, that the correlations at 7 days at the Rock station are weak ($r=0.18$, $r=0.293$). While possible that

the tidal signal is not well-preserved in the Rock record because of the considerable noise observed in the record, a force-balanced modulation of calving behavior would be expected to be recorded at, and thus have a significant correlation with, both stations. It should also be noted that this relationship is problematic because a 7-day lag can only involve about half the data points due to the short duration of the study.

Prioritizing correspondence between the stations, the strongest lag-time correlations are between 1-3 days (r=0.51, 0.46; r=0.58, 0.52; r=0.52, 0.47; with the Delta and Rock stations and for lags of 1, 2, and 3 days, respectively). This matches the three-day lag time shown graphically between the daily high tide level and the calving rate per tidal phase, which illustrates a fairly pronounced oscillatory curve recorded by the Delta station (Figure 17). (A correlation coefficient could not be calculated between the daily high tide and lagging calving rates per tidal phase because of their conflicting timescales.) This relationship would be more strongly supported with corresponding glacier velocity data, which was being studied by researchers at UNIS during the field season but unfortunately was not yet available (Sund, pers. comm., 2010). However, it may be the best explanation of the data given that it yields a common pattern at both the Delta and Rock stations.

The question of why a lag would occur between tidal variations and calving rate has been considered in previous studies, but the answer has not been conclusively determined. One explanation is that tidal changes modulate glacier velocity, and that the tidal wave must travel a substantial distance up the glacier (away from the glacier front) before effecting a velocity change (Thomas 2007; Joughin et al., 2007; Bindschadler et al., 2003; Howat et al., 2007). The relationship between glacier velocity and calving is broadly supported (Benn et al., 2007, Alley et al., 2008, Frezotti, 1997, Haresign and Warren, 2005, Krimmel and Vaughn, 1987, Meier and Post, 1987). Therefore, it may be reasonable to conclude that these two well-supported premises are acting simultaneously, although there is no direct evidence of tidal fluctuations altering the flow dynamics of Kronebreen's glacier terminus.

Various studies have produced mixed results as to whether tidal forcing directly influences calving. Some studies have found that it was a key element controlling calving rates

(e.g., Brown et al., 1982, Legresy et al., 2004, Thomas, 2007, Benn et al., 2007) while others have found no significant influence at their site (Warren et al., 1995, Van der Veen, 2002, O'Neel et al., 2003). This disparity is indicative of the various factors at play. The data presented here support the connection between tidal oscillations and calving rates, but additional study at Kronebreen and in other locations should help to better constrain the effects that tidal changes have on calving.

III. Localizations and Amplitude Inversion

Ability to successfully localize events

The methodology used for localizing unobserved calving events was effective in utilizing the available data from the tide gauges, but contained broad uncertainties. The estimating models- Deep Water/Transitional (at 50m, 30m, and 20m wavelengths) are quite rough, both in using an average depth rather than variable-depth for the initial calculations and also because a single wavelength is assumed for all events since data on the wavelengths for each event could not be elucidated. The Deep Water/Transitional calculations are only valid if the wavelengths of most events are approximately the same size, which could not be confirmed by this study. Shallow water approximations are normally used when water depth is less than 1/20 of the wavelength. Table 3 shows the average depth across each transect, taken from the bathymetry data collected by Laura Kehrl (Kehrl, 2010) (Figure 4).

Considering the complexity of accurately modeling wave patterns, the most promising estimation comes from the calculated boundaries based on the analysis of paired events (events both visually observed and recorded by a tide gauge, giving a known calving time to compare with the arrival time of the wave signal). These estimates resulted in the Real-mean and Real-zoneadd boundary limits included with the other models in Table 4, and had the closest correspondence to the data from visually observed events (see Table 13). However, these

estimates still contain considerable uncertainties as a result of the relatively small sample of paired events recorded by the loggers at both stations.

Zone-specific calving size estimates

By interpreting the sources of the calving events, other conclusions can be drawn assessing the calving behavior of different zones of the glacier front. Three spatial assessments of calving volume have been considered: first, the subjective calving sizes for visually observed events (Figure 25); second, the recorded wave amplitudes for paired events (Figures 23, 24); third, the inverted wave amplitude for PEs (Figure 26). The assessments concur in that zone 4 is recognized across each record as a source of large-amplitude waves, and by inference, large calved icebergs. The visual data and paired events from the Rock station both show high-amplitude waves from zone 1-2, and the Deep Water/Transitional (50m and 20m) models and the Real data-zoneadd model both show high average wave amplitudes for events originating in zone 3-4.

Zones 2 and 4 both contained embayed segments along the ice front, and have been recognized as regions of high calving (see Figure 1) (Trusel et al., 2010). Therefore, it makes sense that high rates and volumes of calving would occur in these regions, and the confirmation of these regions of high calving by various estimation methods also helps validate these estimates.

Interpretations from inverted amplitude data

An odd element that becomes apparent when considering the inverted amplitude data is that in many instances, the Rock Station and Delta station values do not yield identical estimates, and are sometimes widely different. Since the estimates are for PEs and should be estimating the size of a single event, the original wave amplitude should be very similar. In many instances, even in which the amplitudes recorded at each station are quite different, the estimated original

amplitude is within 1m difference. In others, the difference is as large as the difference between the two original values, and in a few, the difference in the estimates of the original amplitudes are greater than the differences in the wave signals received at the two tide gauge stations.

There are a few interpretations of this trend. The concurrence of the predicted signals could be used to determine whether the model being used to localize the event is appropriate. This is contradicted, however, by the relationship shown in Figure 27 between the zone of the originating event and the difference in the estimated original wave amplitude. This shows that events coming from the center of the glacier front tend to yield similar estimates from both stations, while events with larger estimates by the either the Rock or Delta station tended to originate far from it. This indicates that the calculation of the attenuation does not effectively deal with waves traveling long distances (>2km). It could also be pointing towards the site-specific differences in the recording of wave amplitude that have been noted throughout this study, particularly that the overall reception at the Rock station is considerably larger, likely due to the bathymetric and geometric differences in the areas surrounding each station.

IV. Comparison with other calving loss monitoring methods

While no published studies have used tide gauges to study calving at Kronebreen/Kongsvegen, a number of studies have used other methodologies to do so. Sedimentological approaches have considered bed landforms in the context of past terminus positions (Glasser and Hambrey, 2001) and others have analyzed the character of the iceberg bits being produced (Dowdeswell and Forsberg, 1992). Sund and others (2008) used photogrammetry to monitor the volume of ice being lost at the front of Kronebreen in coordination with the glacier flow velocity. This methodology does not consider short-term changes but rather deals with the larger patterns of ice loss. This methodology is especially useful in estimating the total volume of ice lost over a period of months or years. Another study conducted recently used radar imaging to attempt to monitor large calving events at Kronebreen, and past studies have used this method as well (Lefauconnier et al., 1994; Rolstad and Norland, 2009). This approach

has met mixed success, but primarily seems to be effective at estimating the volume of individual events, although the size must be sufficiently large to be identified by the radar. Unfortunately, logistical limitations prevented direct, simultaneous comparisons of the approach used in this study with the alternative methods noted above.

CONCLUSIONS

This study, while somewhat inconclusive, provides several key observations and recommendations for future calving studies.

- Tidal fluctuations are shown to have significant influences on calving rate, as well as total ice lost (taken from the indicator of average or maximum amplitude over a given interval). The observation of lag times between tidal oscillation and calving add complexity to the scenario, however.
- Air temperature shows a substantial but not statistically significant relationship with calving, especially with the measures most representative of ice mass loss, indicating that temperature may play a role in controlling the occurrence of larger calving events.
- Localization of calving events can be approximated based on a two-station setup, although the uncertainty associated with the estimates is large. A three-station approach is recommended for future years.
- This project confirms several relationships observed in previous studies (Brown et al., 1982, O'Neel et al., 2001) regarding the connection between environmental variables and calving, and finds stronger relationships between tidal oscillations and calving than in some previous studies (Warren et al., 1995, O'Neel et al., 2003).

- Compared with previously published attempts to study calving in Kongsfjorden, a water depth/pressure logger allows for the most effective monitoring of glacial calving processes over short time scales.

The baseline data established in this study should be expanded upon in future research and years of the Svalbard REU. Comparison of the rates observed during this melt season with those of previous and future melt seasons, as well as including additional external factors, especially glacier terminus velocity, could reveal intriguing connections underlying the periglacial environment at Kronebreen-Kongsvegen.

SPECIFIC RECOMMENDATIONS FOR FUTURE WORK

Monitoring calving by water depth/pressure loggers shows good potential for future inquiry, but there are some changes to methodology that would make the data retrieval more efficient and the data more reliable. The most useful changes would be in the implementation and deployment of the water depth/pressure loggers. Both of the stations chosen for the study met their two primary objectives: the gauges received the calving wave signals and were not damaged by an iceberg. Therefore, considering that each is approximately as close as possible to the ice front, station locations should likely be retained, despite the non-symmetrical amplitude reception at the two stations. However, one of the most inconvenient aspects of data analysis was the movement of the water depth/pressure logger station laterally along the fjord floor, causing frame-shifts that required a time-consuming correction process and introduced uncertainty into the dataset. A stabilizing construction that more securely anchors the gauge in place could decrease the number of this type of vertical frameshift data artifacts.

An additional problem was the limited battery life and data recording space on each water depth/pressure logger. This is more difficult to resolve because it involves one or both of a remotely deployed battery/generator and data storage memory unit to collect data over longer,

continuous intervals. Lacking this option, the water depth/pressure loggers should be collected more conservatively, leaving no periods between the end of the recording period and the beginning of the next, i.e., a break between the stop time of the recording space and the collection time of the instrument during the day. This could be resolved by having twice as many water depth/pressure loggers as need to be deployed, allowing each to be replaced at the end of each day.

Further exacerbating the problem of too-short sampling periods is the additional recommendation of higher frequency sampling, with a 2-5 second sampling interval appearing optimal. While the number of calving events was accurately recorded by the 10-second sampling period utilized for most of this study, the calving event wave periods are sometimes shorter than ten seconds, and a shorter sampling interval would allow for more detailed analysis of the waveforms (for instance, frequency analysis as performed by Iizuka et al., 2004) and for better identification of the initial arrival and duration times of each wave sequence.

A final recommendation regarding the water depth/pressure logger deployment is for a third water depth/pressure logger station, although the potential location of the station is uncertain as deployment in the center of the fjord is problematic for logistical reasons. A third water depth/pressure logger would make triangulation of the source of each event much more accurate.

A recommendation for future study not regarding water depth/pressure loggers is the collection of additional peripheral data. For instance, constant-depth CTD casts could be drawn along transects parallel to the glacier front at regular temporal intervals over the study period and these data could be compared with calving rates. This is an important consideration, since variable salinity has been proposed as an explanation for observed differences in calving rates, and this year a very high salinity Atlantic Water layer was detected in multiple CTD casts in the central fjord (Marshburn, 2010). Variations in fjord water flow might be detected temporally and spatially that could shed insight onto the patterns of calving not otherwise explained in this study (Nilsen et al., 2008).

FIGURES

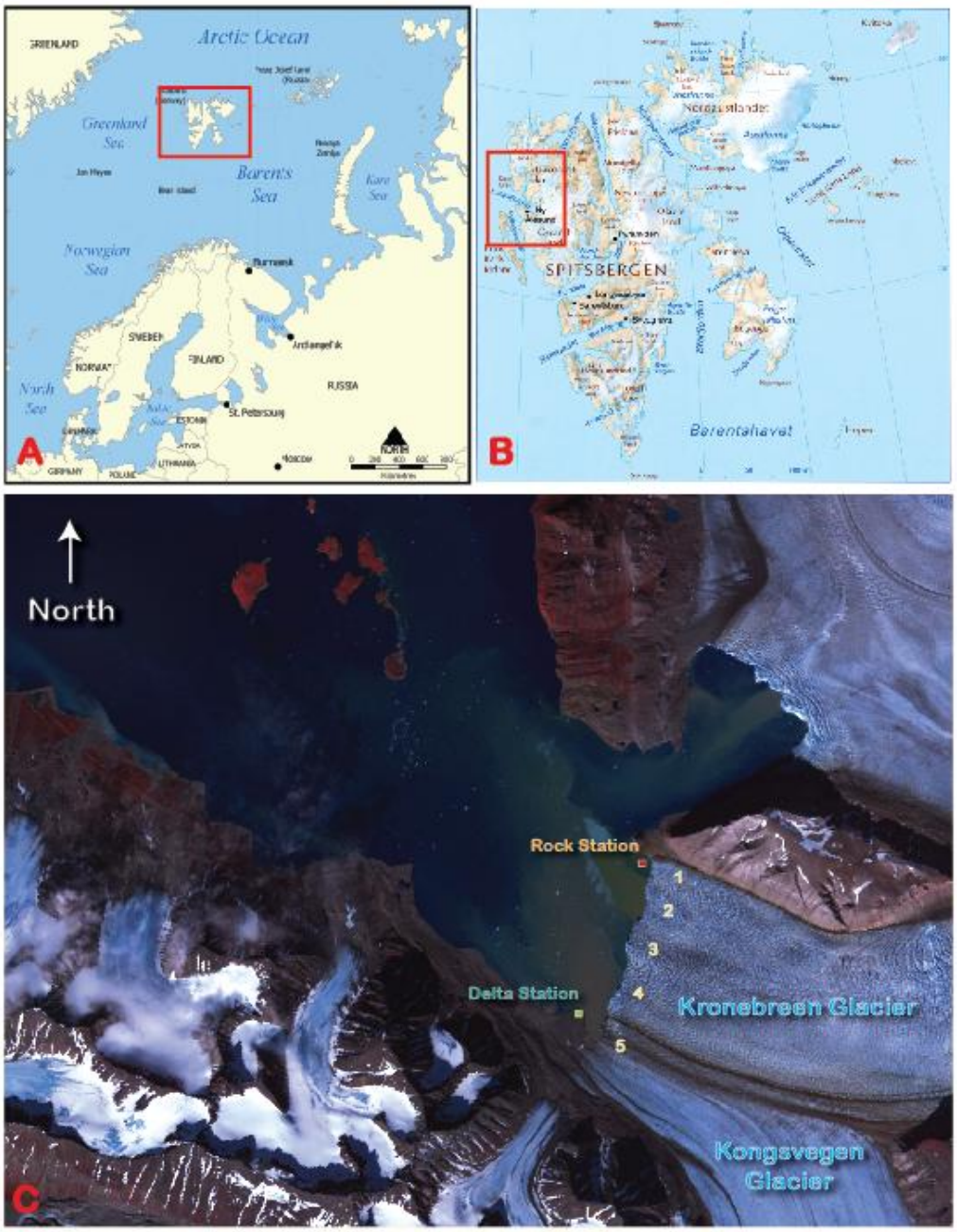

Figure 1. Maps of (A) the Barents Sea region of the Arctic and North Atlantic, (B) the Svalbard archipelago, and (C) southern Kongsfjorden, Spitsbergen, Svalbard, including outlets of Kronebreen and Kongsvegen glaciers. Both water depth/pressure logger stations are labeled, as are the Zones described for purposes of approximate localization of calving events.

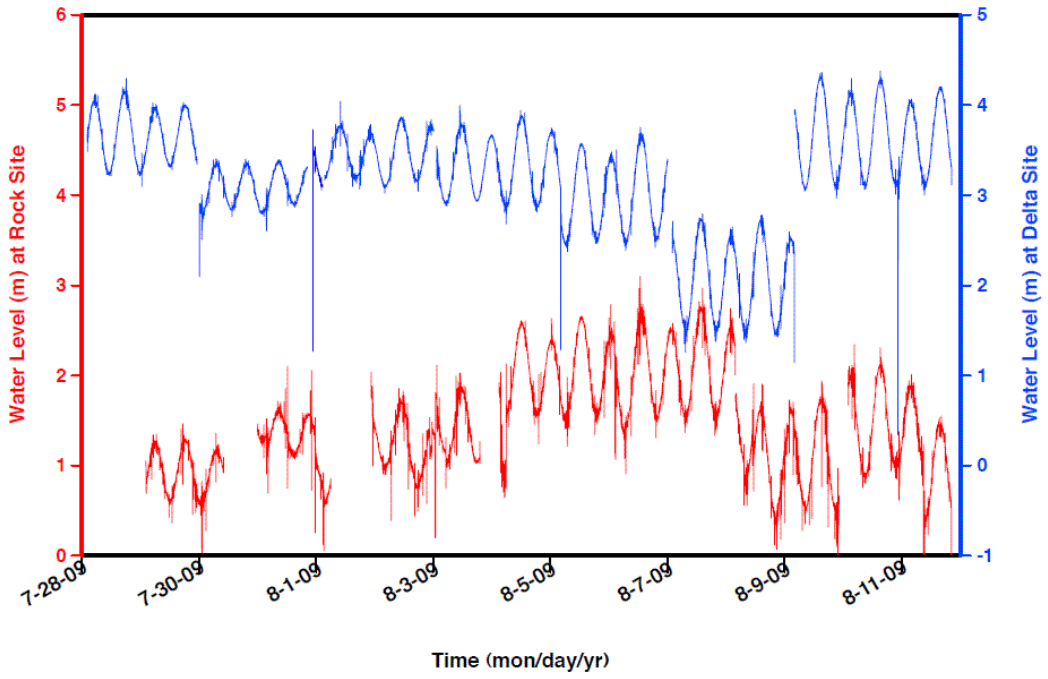

Figure 2. Raw water level data from water depth/pressure loggers proximal to Kronebreen-Kongsvegen ice front. Water level (depth) is the difference between the bottom-anchored pressure sensor and the water surface. Trailing ends are artifacts of the gauge being out of the water at that time and these regions were removed from the dataset for analytical purposes.

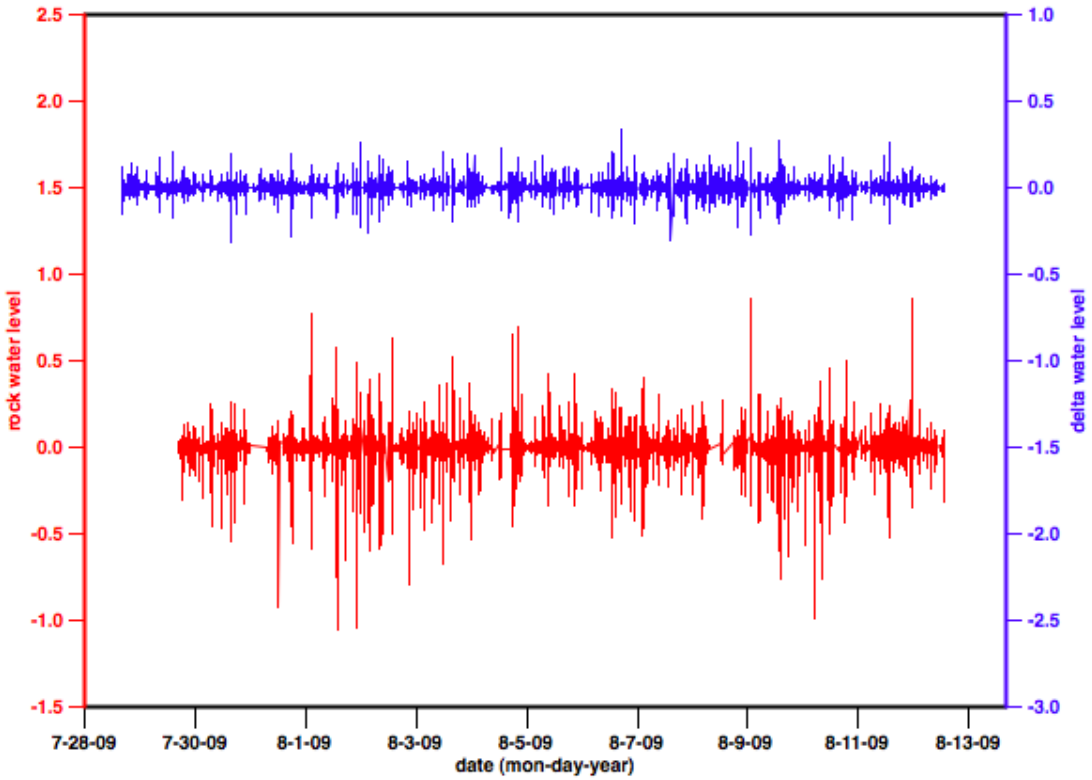

Figure 3. Adjusted water level data from water depth/pressure loggers proximal to Kronebreen-Kongsvegen ice front. Water level depth values are comparable between stations, but represent a value relative to the Ny Ålesund weather station tidal standard, not necessarily actual water depth. The data are not shown with amplitude adjustments, which can only be calculated for individually identified calving events and not the full spectrum.

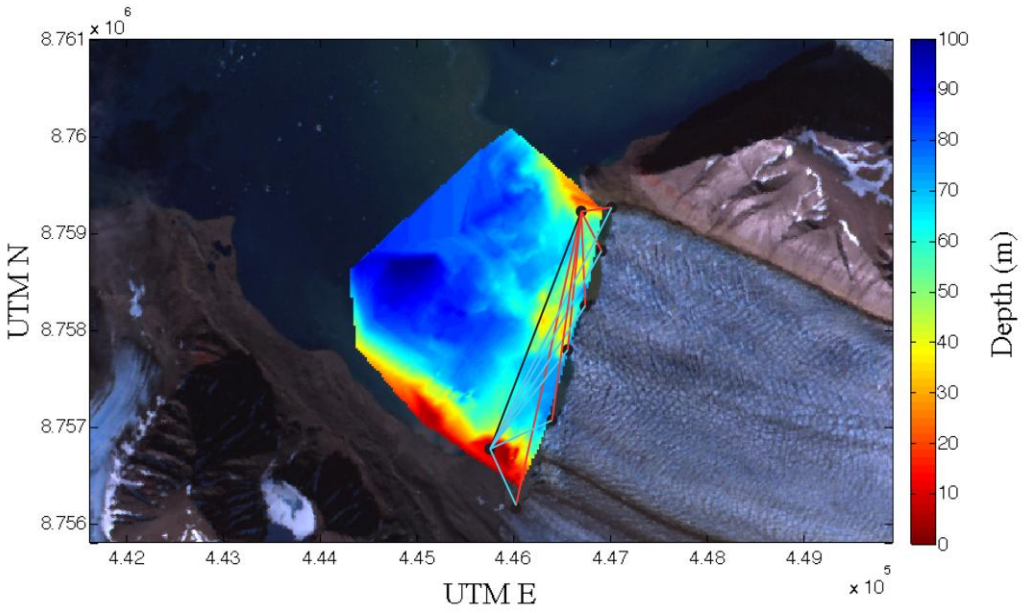

Figure 4. Shaded bathymetric image (Kehrl, 2010) with superimposed lines connecting water depth/pressure logger mooring stations with structural zone borders of the glacial front. The average depth over these transects was estimated for input into the expected travel-time equations (blue transects are between the Delta, red between the Rock). See Table 1 for the summary of the transect data.

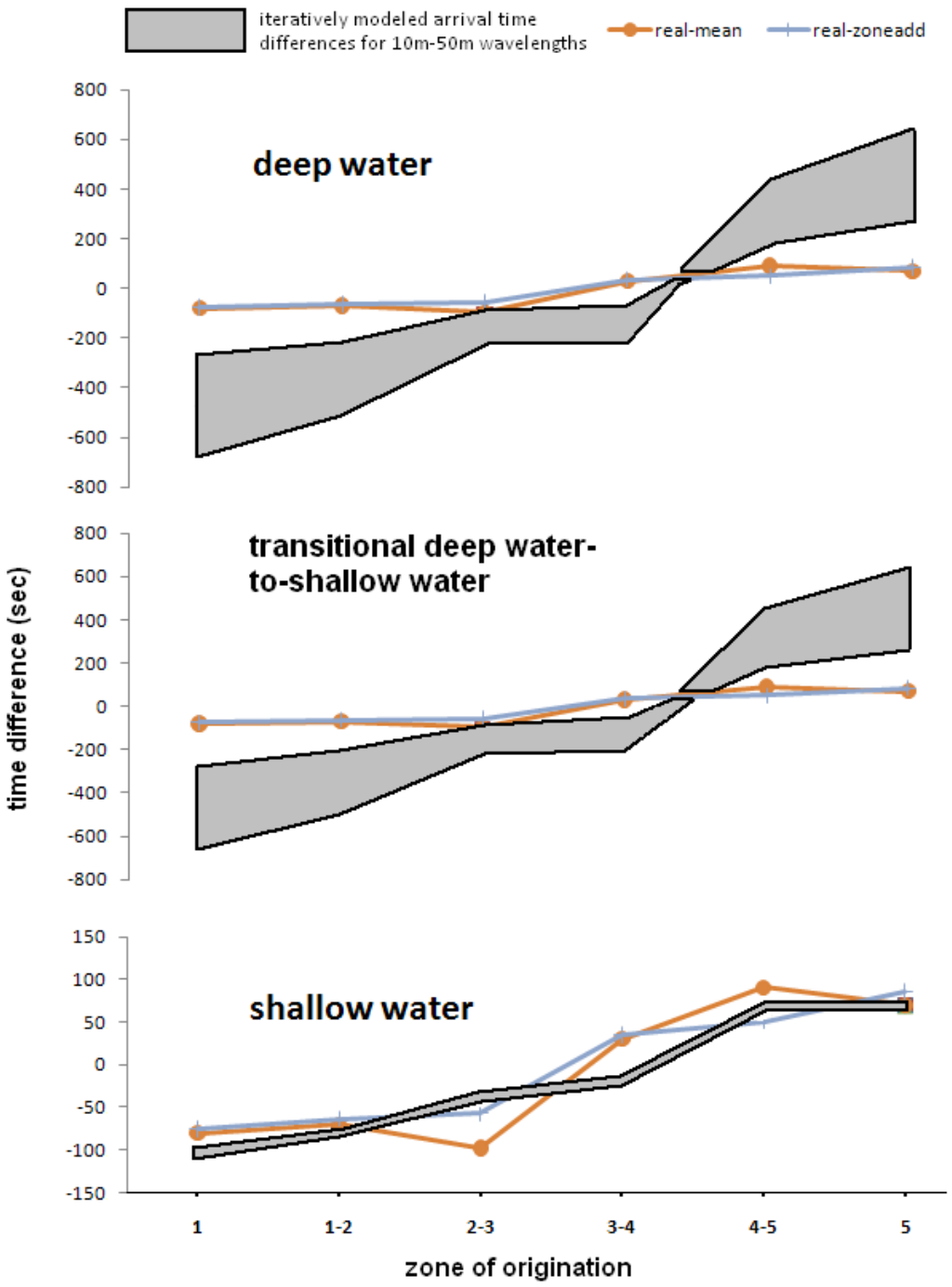

Figure 5. Modeled and observed arrival time differences of deep water, shallow water, and very shallow water surface wave simulations at varied wavelengths and sourced to different zones. Wave equations listed in Methods and transects calculated in Table 2. "Real-mean" is the mean value observed in events both observed and recorded by the water depth/pressure loggers at that zone section. "Real-zoneadd" is the mean of the zone and each bordering it (e.g., "zone 1-2" averages events from zone 1, zone 1-2, and zone 2). Legend shows wavelengths in meters.

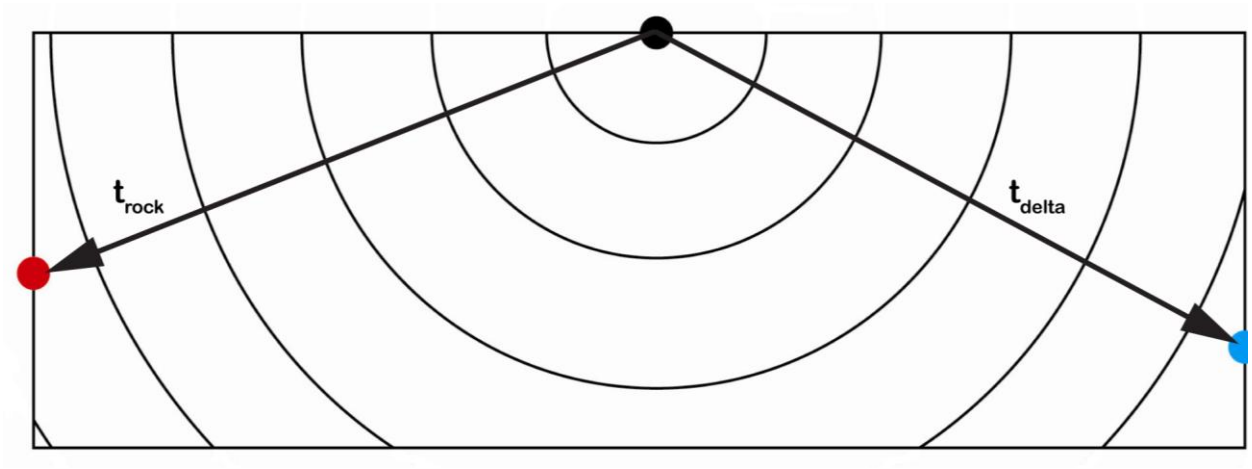

Figure 6a. Theoretical diagram of wave propagation from a calving event at the glacier front. All things being equal, events originating equidistant from both stations should theoretically arrive at the same time, leading to the zero (0) time difference shown in Figure 5.

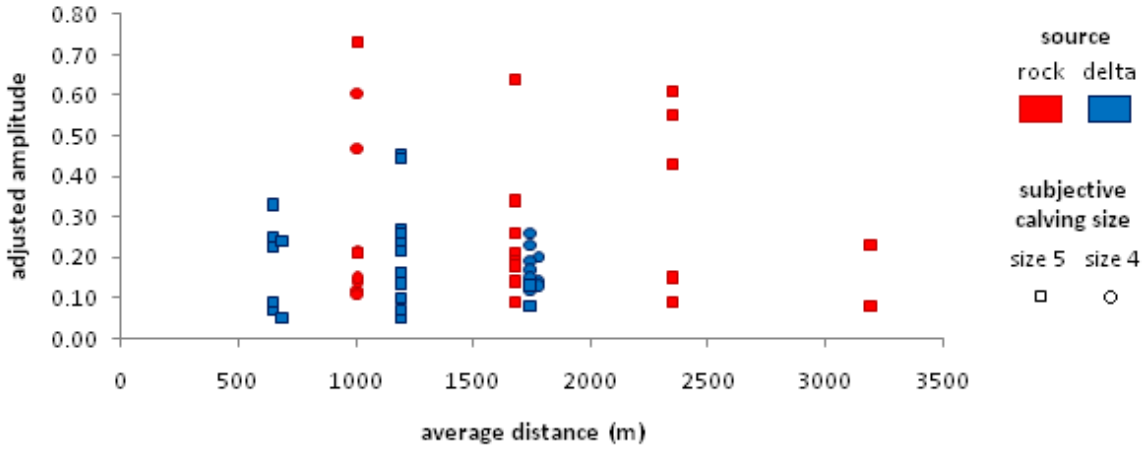

Figure 6b. Wave travel distance vs. adjusted wave amplitude for largest paired events. Average distance is the mean travel distance from a given source zone. Only events with a subjective size of 4 or 5 (out of 5) were included. The generally decreasing amplitude with greater travel distance for events of a known visual size is the expected attenuation pattern described by equation 6.

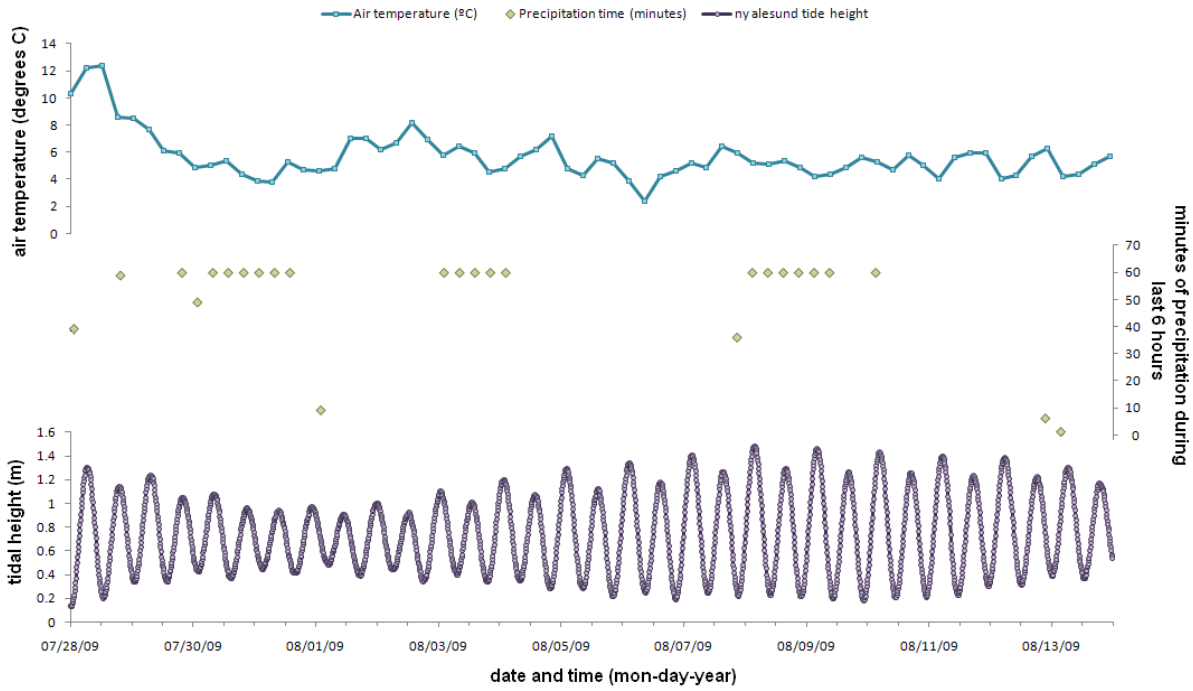

Figure 7. Air temperature, precipitation, and tidal data from Ny Ålesund. Collected by and obtained from Norwegian Meteorological Society (met.no) at Ny Ålesund, Svalbard.

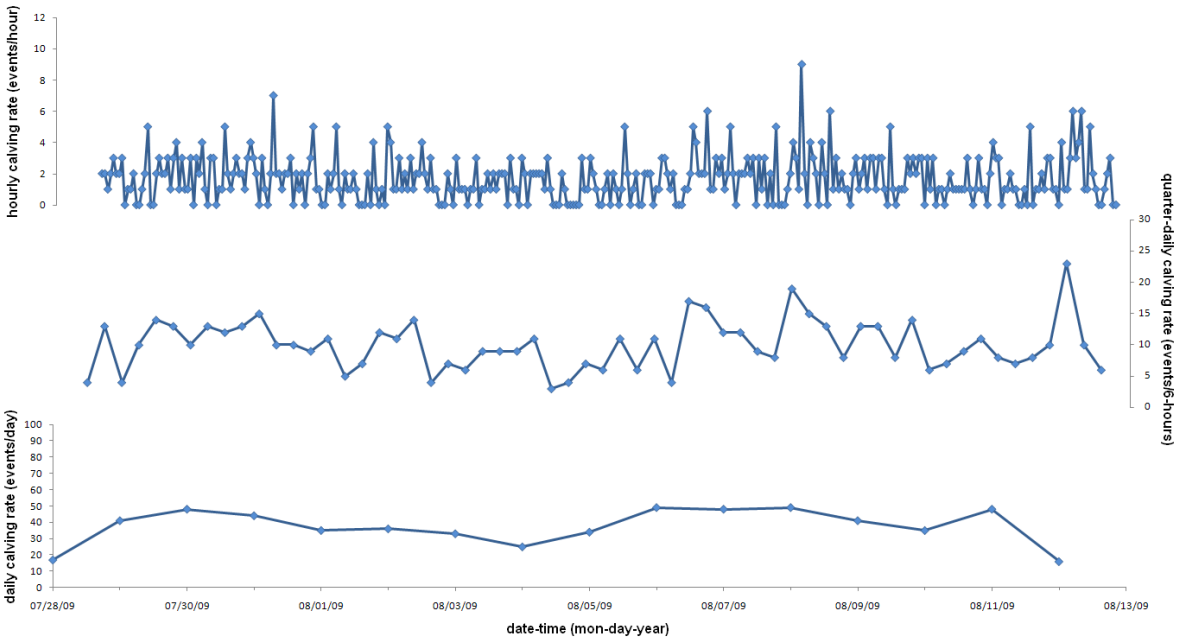

Figure 8a. Calving rates recorded by Delta water depth/pressure logger on hourly, quarter-daily, and daily timescales**.**

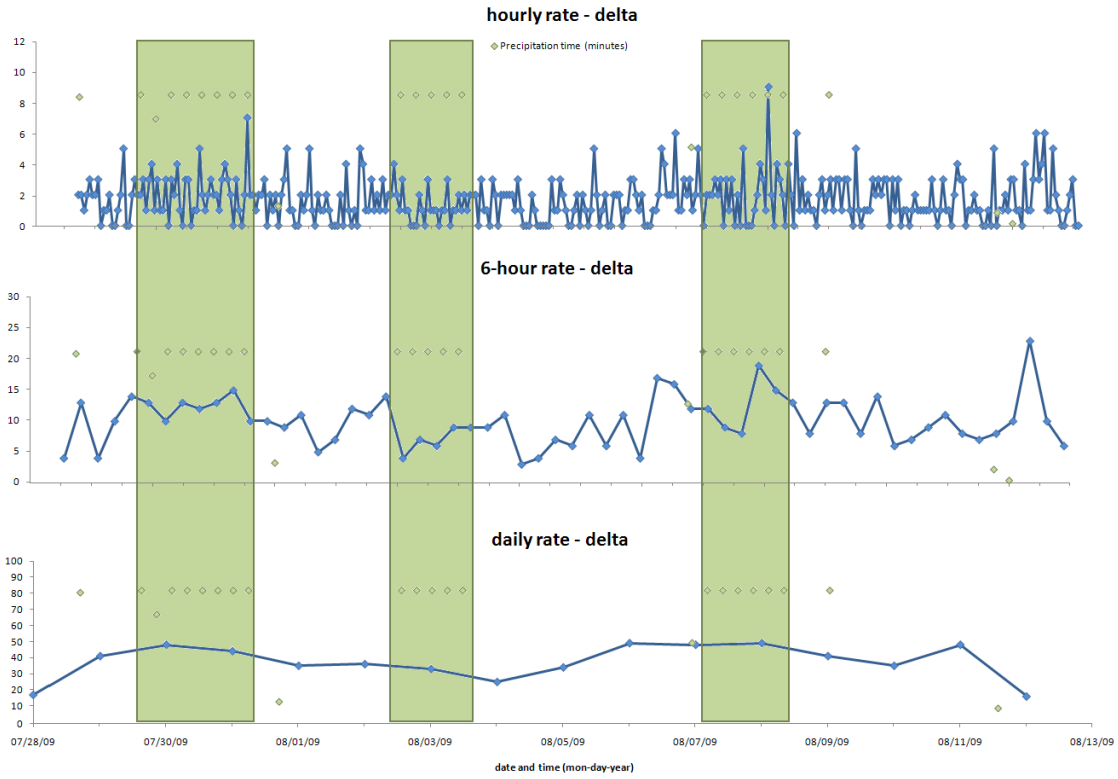

Figure 8b. Hourly, quarter-daily, and daily calving rates at the Delta station, with precipitation time during the last hour plotted for comparison.

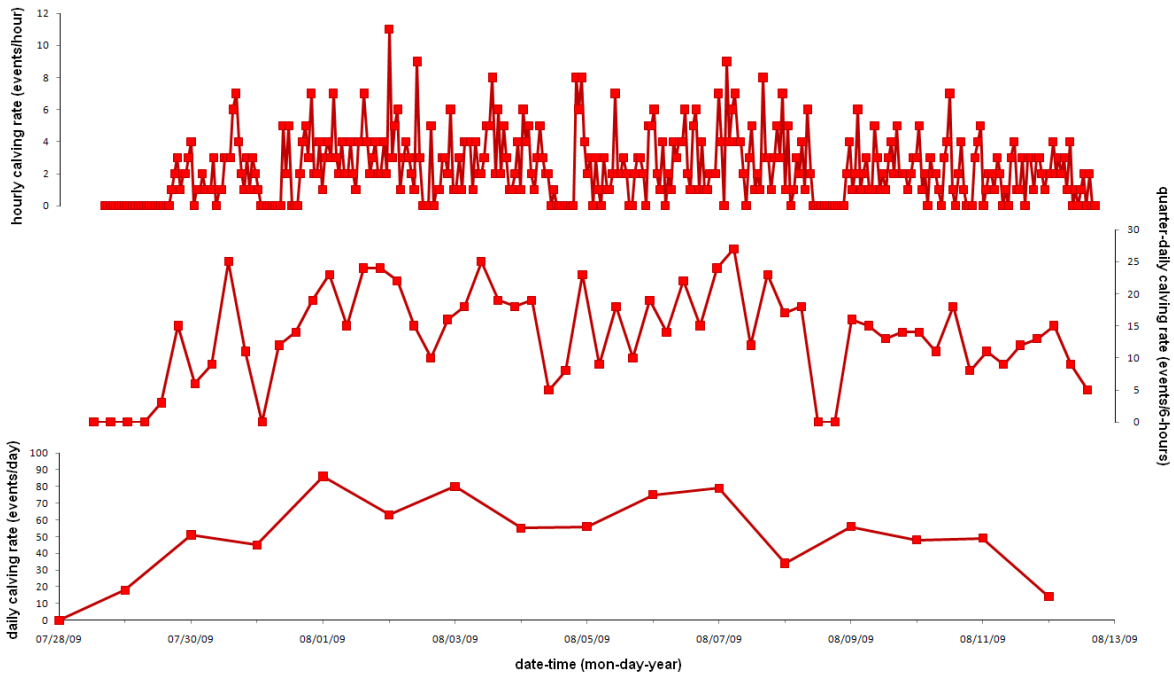

Figure 9a. Calving rates recorded by Rock water depth/pressure logger on hourly, quarter daily, and daily timescales.

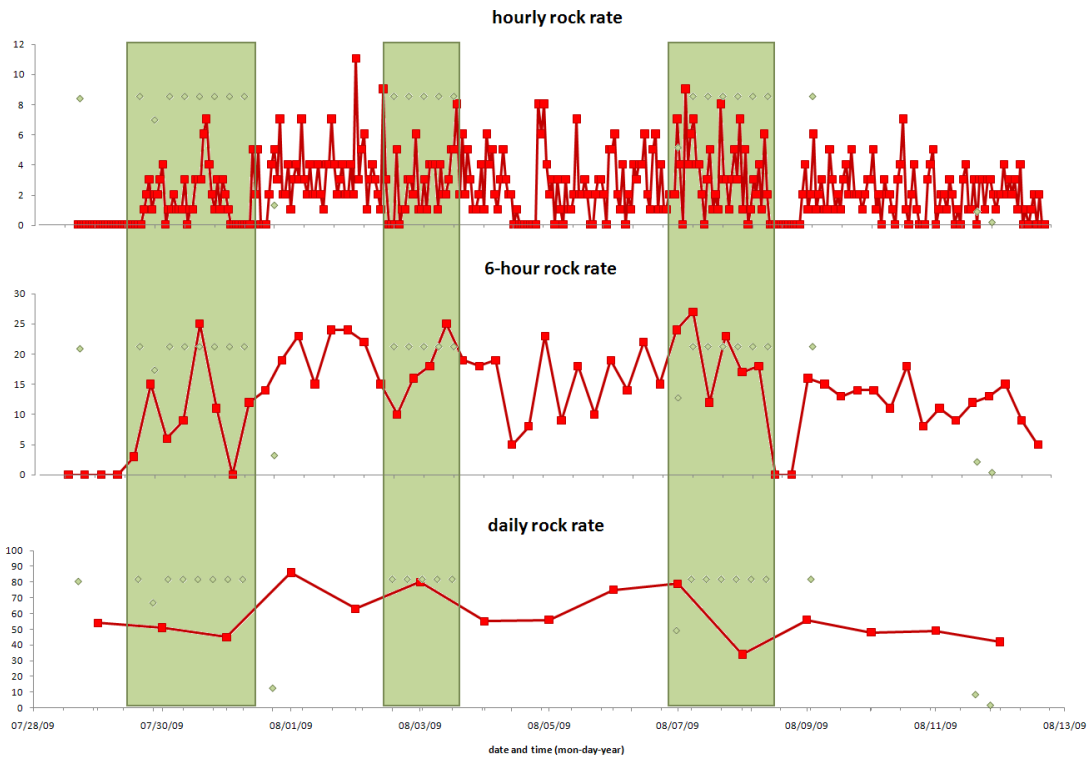

Figure 9b. Hourly, quarter-daily, and daily rates of calving at Rock station, with precipitation time during the last hour plotted for comparison.

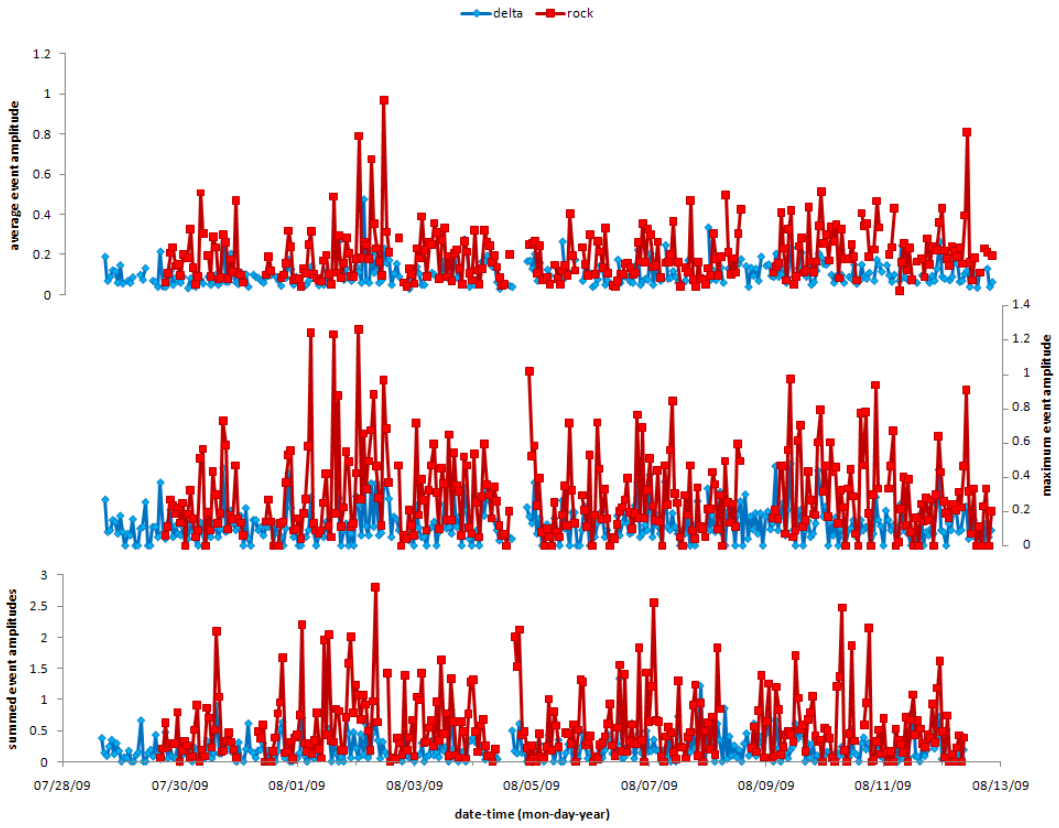

Figure 10. Measures of calving event amplitudes over hourly timescales.

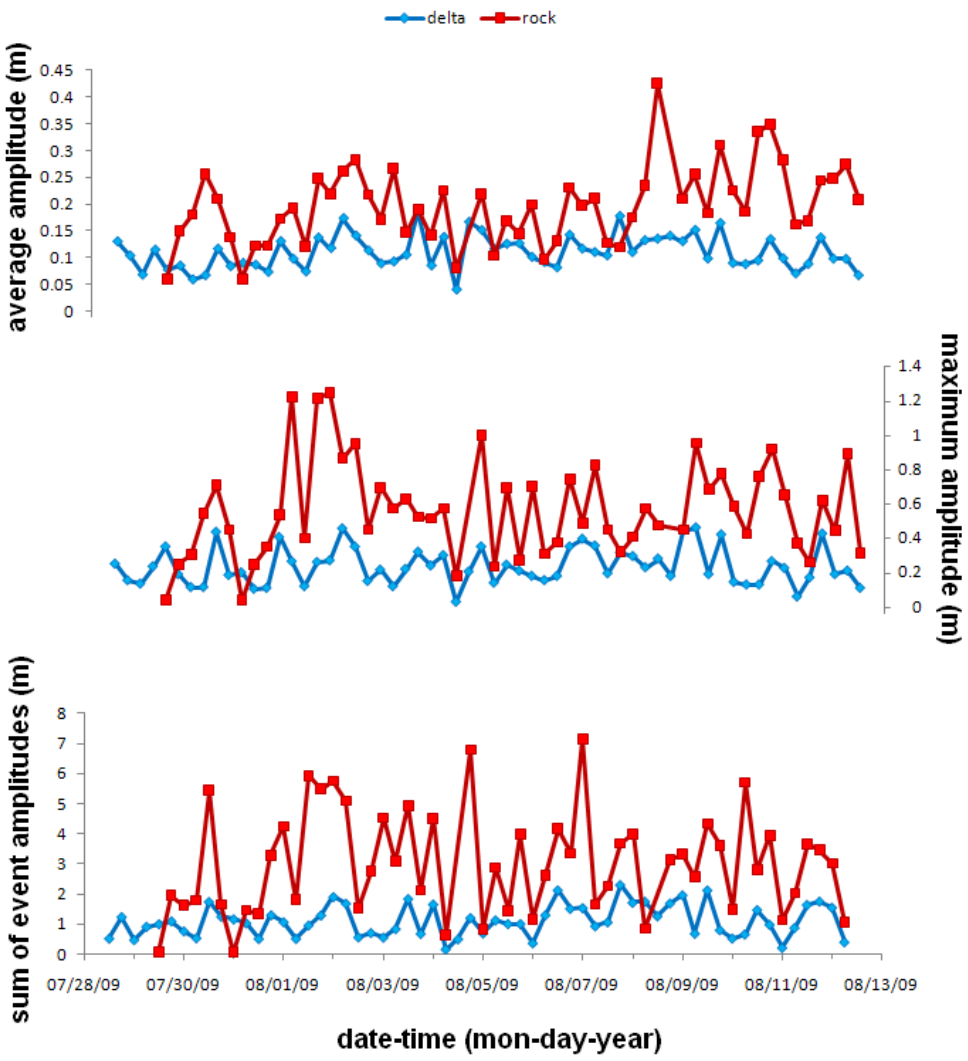

Figure 11. Measures of calving event amplitudes over quarter-day (6-hour) timescales.

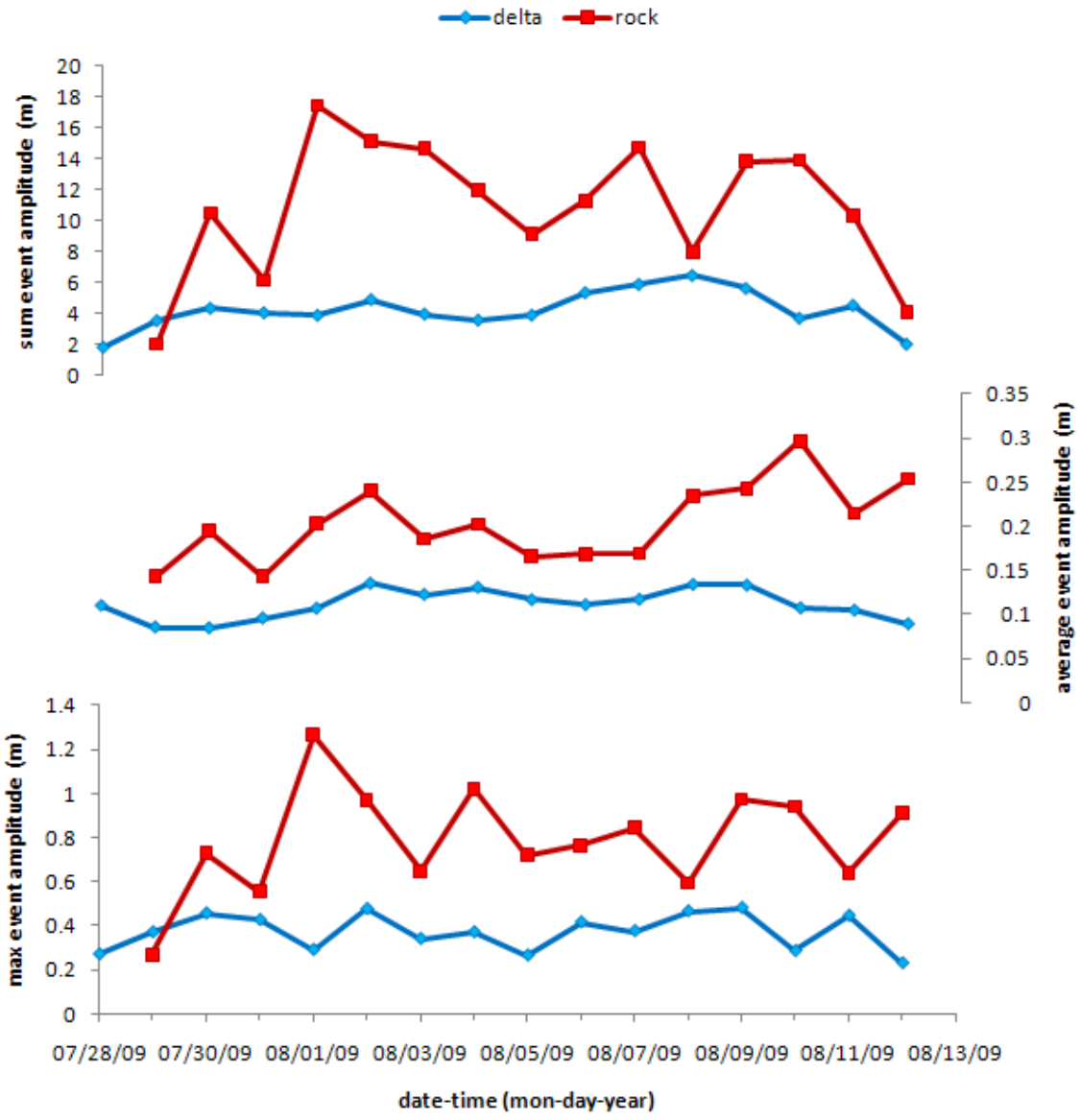

Figure 12. Measures of calving event amplitudes over daily timescales.

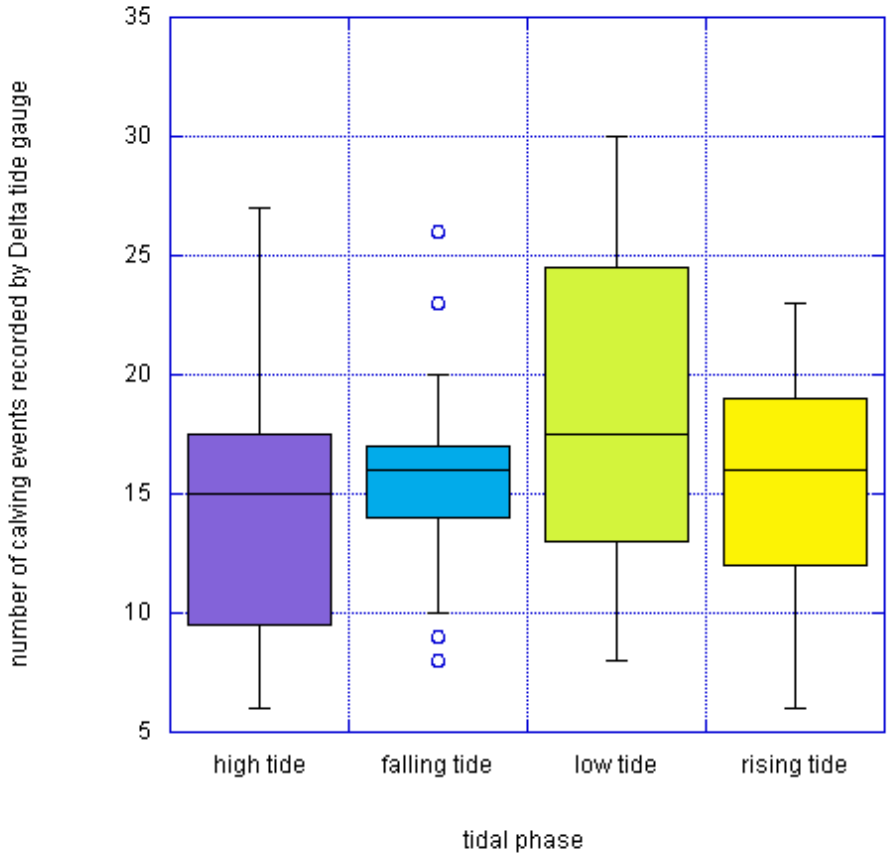

Figure 13. Number of calving events recorded during each tidal phase as recorded by Delta tide gauge station. The central black lines in each box represent the mean, the extent of the box represents the distance to one standard deviation, and the bars outside the box represent the extent of the second deviation. Dots outside the box indicate the existence of outliers beyond the second standard deviation.

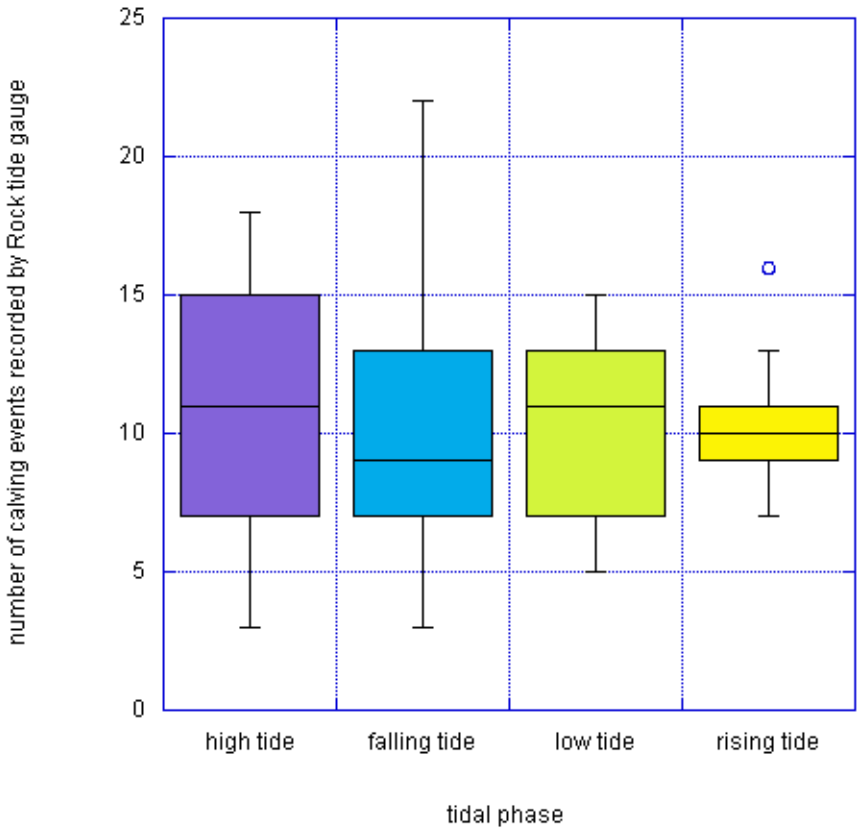

Figure 14. Number of calving events recorded during each tidal phase as recorded by Rock tide gauge station. The central black lines in each box represent the mean, the extent of the box represents the distance to one standard deviation, and the bars outside the box represent the extent of the second deviation. Dots outside the box indicate the existence of outliers beyond the second standard deviation.

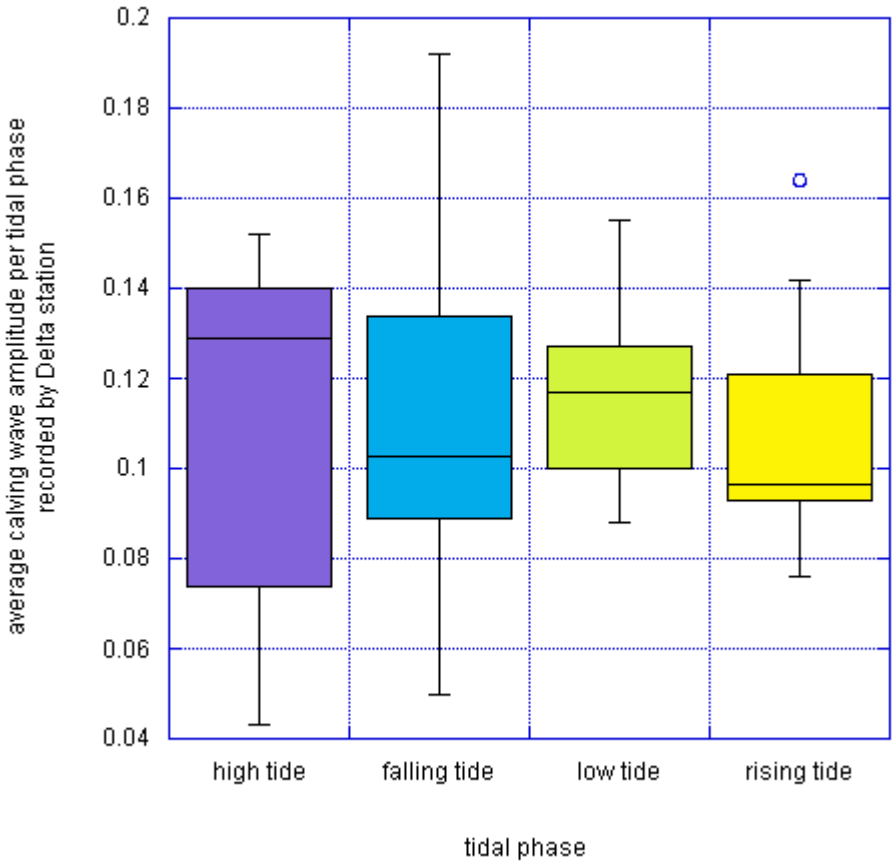

Figure 15. Average calving wave amplitude during each tidal phase as recorded by Delta tide gauge station. Wave amplitudes were averaged for identified calving events over the once-daily tidal phase duration. The central black lines in each box represent the mean, the extent of the box represents the distance to one standard deviation, and the bars outside the box represent the extent of the second deviation. Dots outside the box indicate the existence of outliers beyond the second standard deviation.

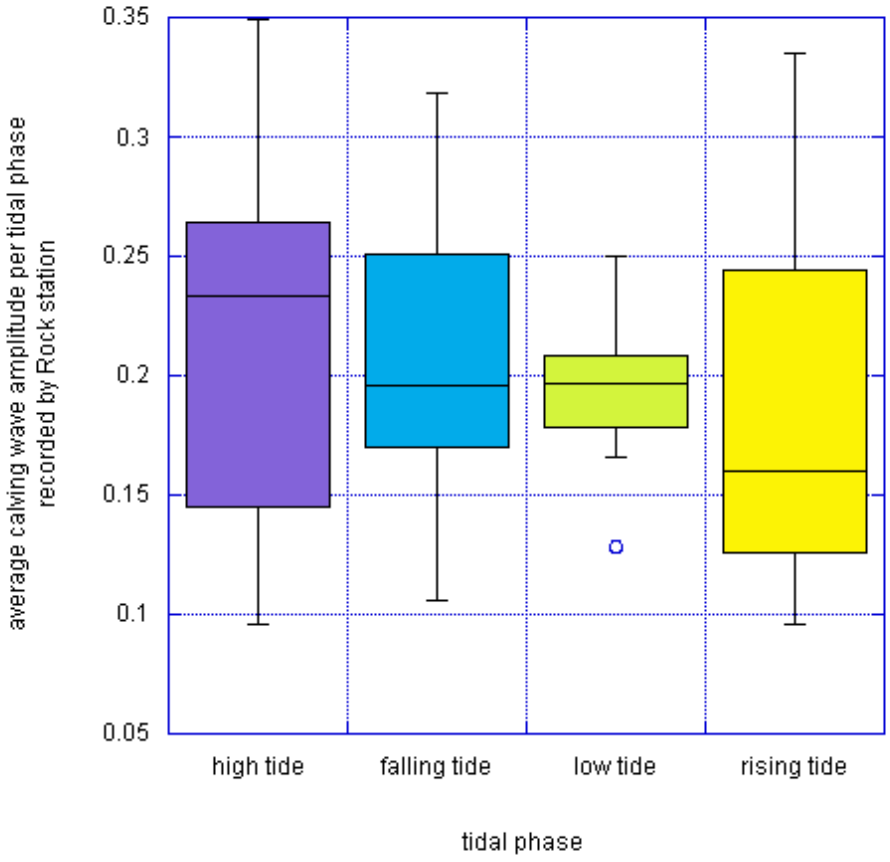

Figure 16. Average calving wave amplitude during each tidal phase as recorded by Rock tide gauge station. Wave amplitudes were averaged for identified calving events over the once-daily tidal phase duration. The central black lines in each box represent the mean, the extent of the box represents the distance to one standard deviation, and the bars outside the box represent the extent of the second deviation. Dots outside the box indicate the existence of outliers beyond the second standard deviation.

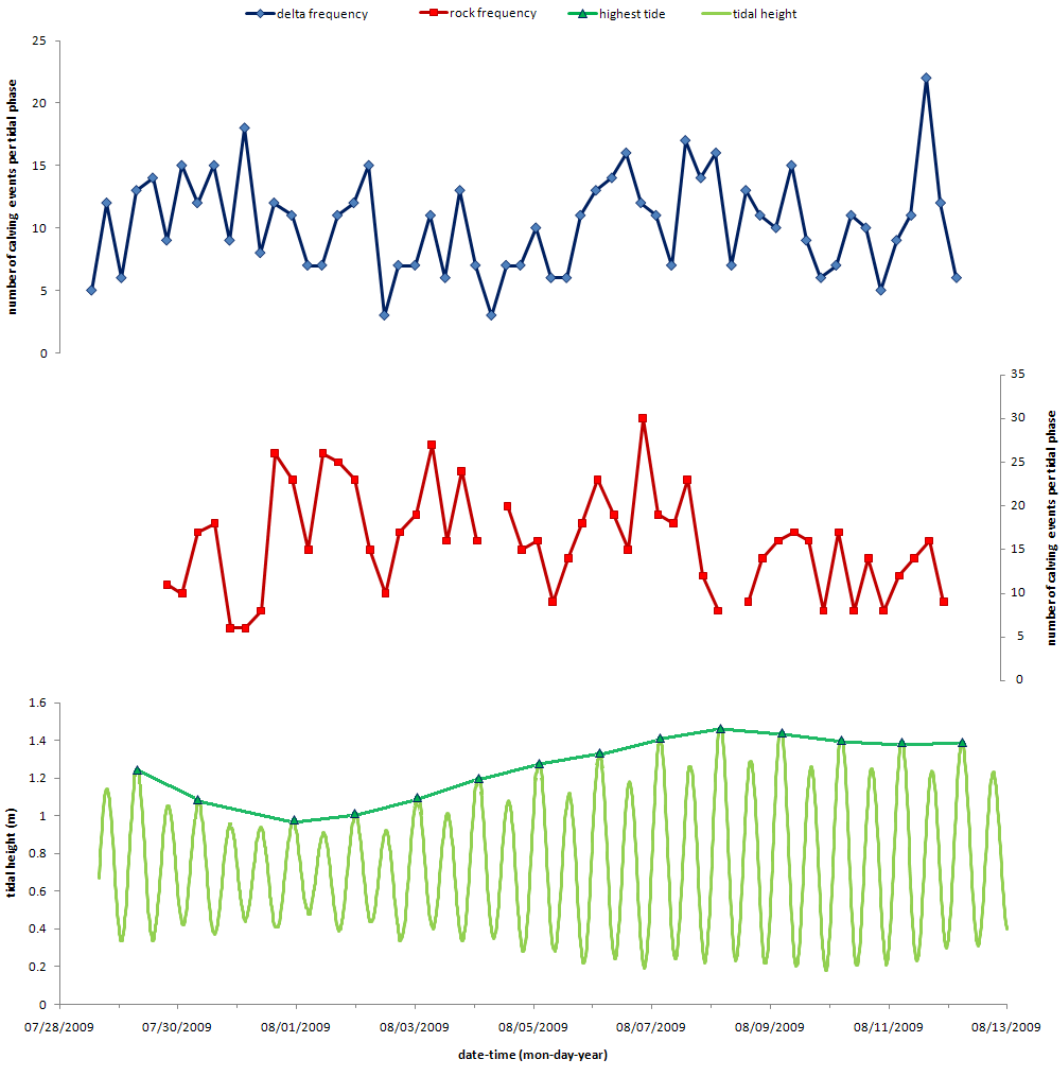

Figure 17. Calving rates per tidal phase at Delta and Rock stations, with tidal oscillation and high tide level.

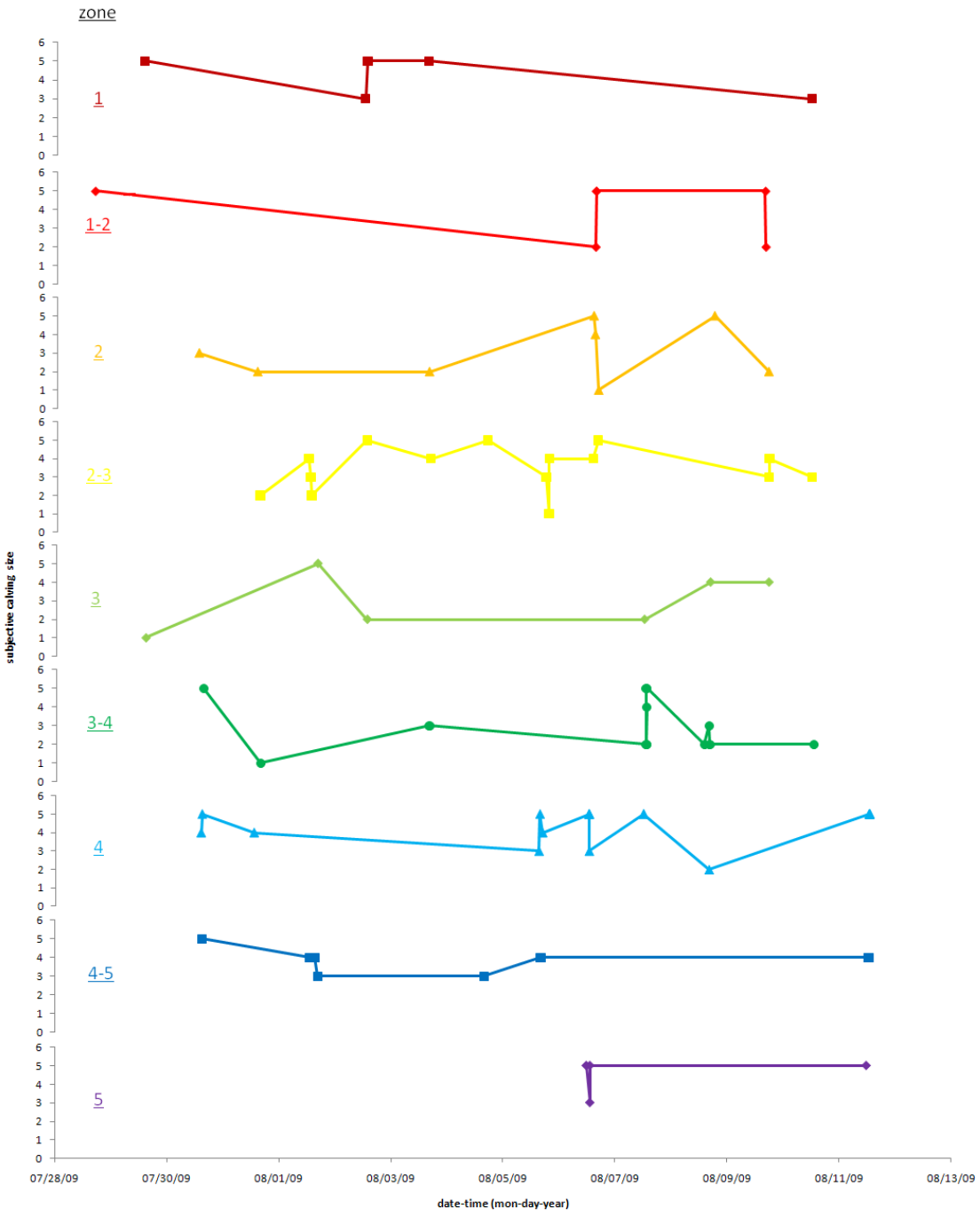

Figure 18. Subjectively determined size of visually observed calving events within each of the define zones of the glacier front, as shown in Figure 1.

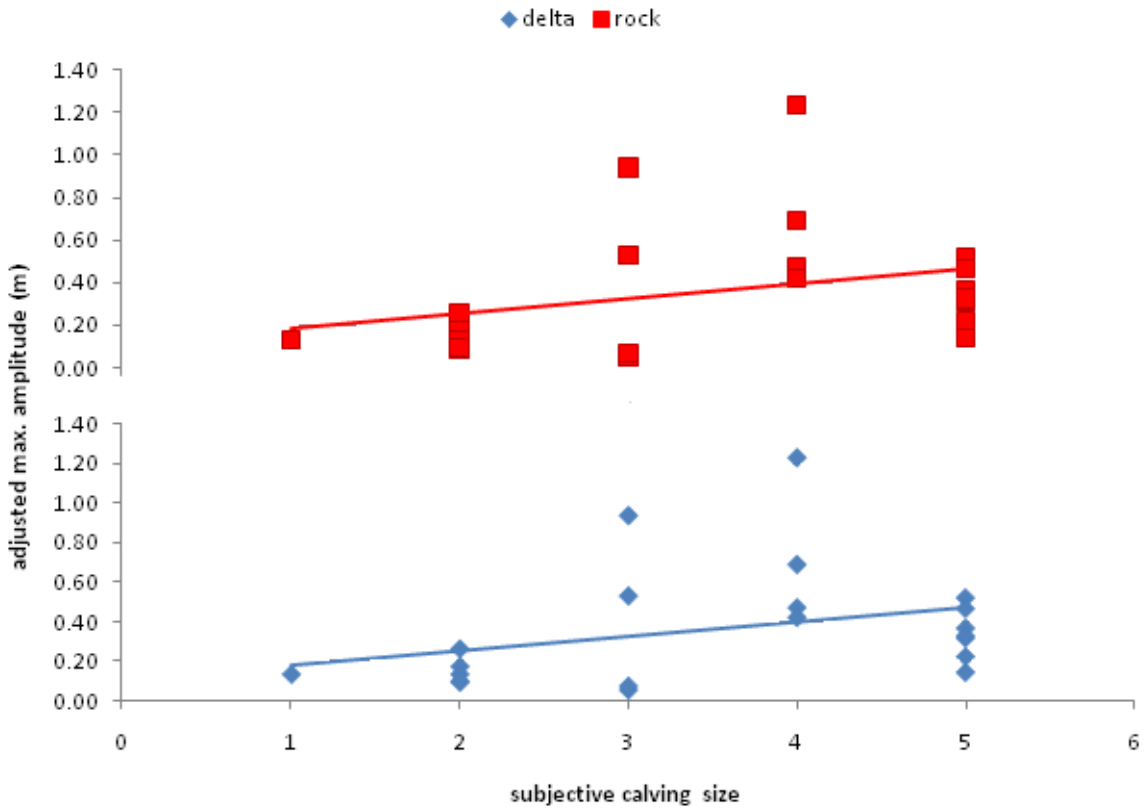

Figure 19. Subjective calving event size vs. maximum adjusted wave amplitude recorded by pressure loggers. Compares only events both visually observed and electronically recorded.

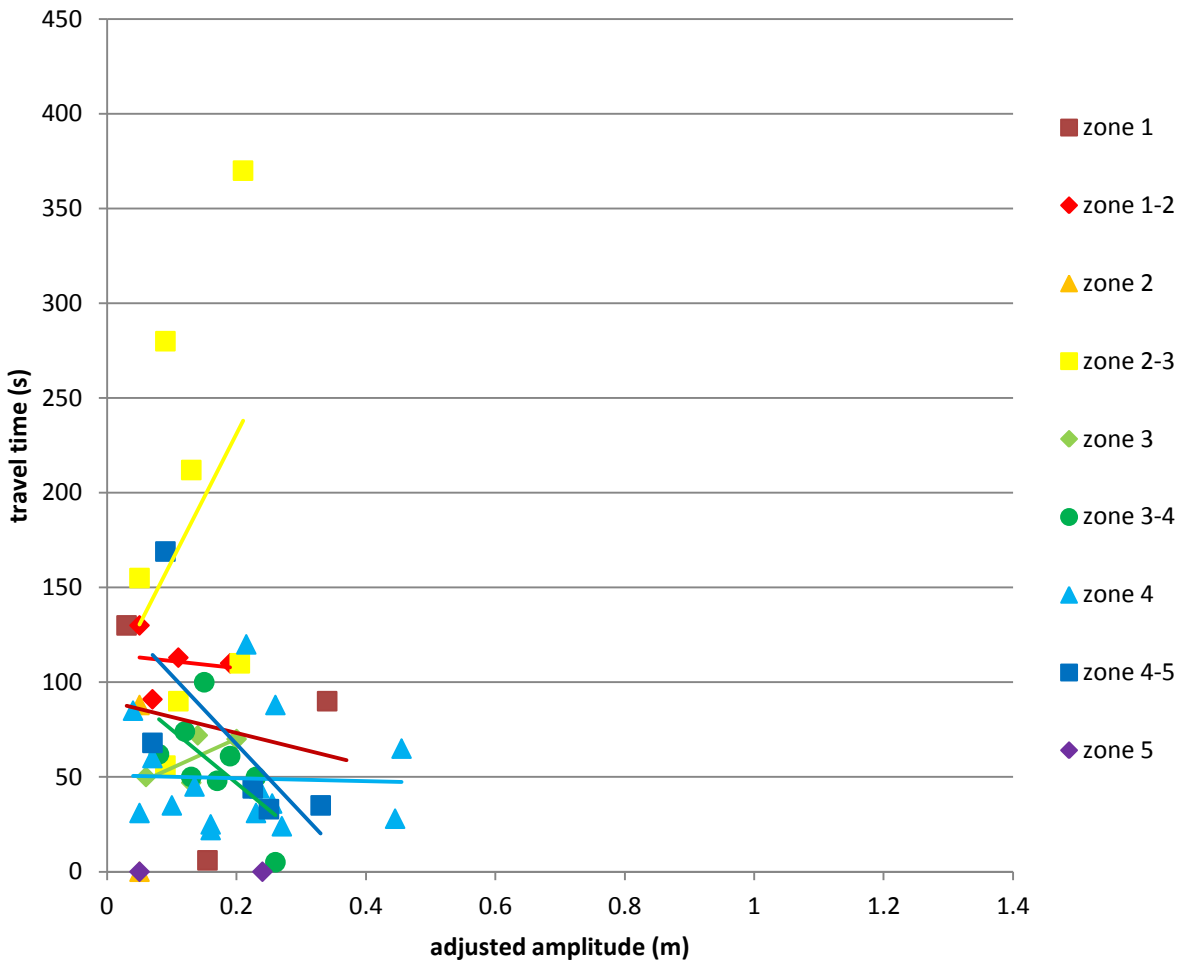

Figure 20. Delta station: Adjusted amplitude vs. wave travel time. Data points are exclusively events both visually observed and electronically recorded (paired events). Linear regression equations modeling this relationship are shown in Table 11.

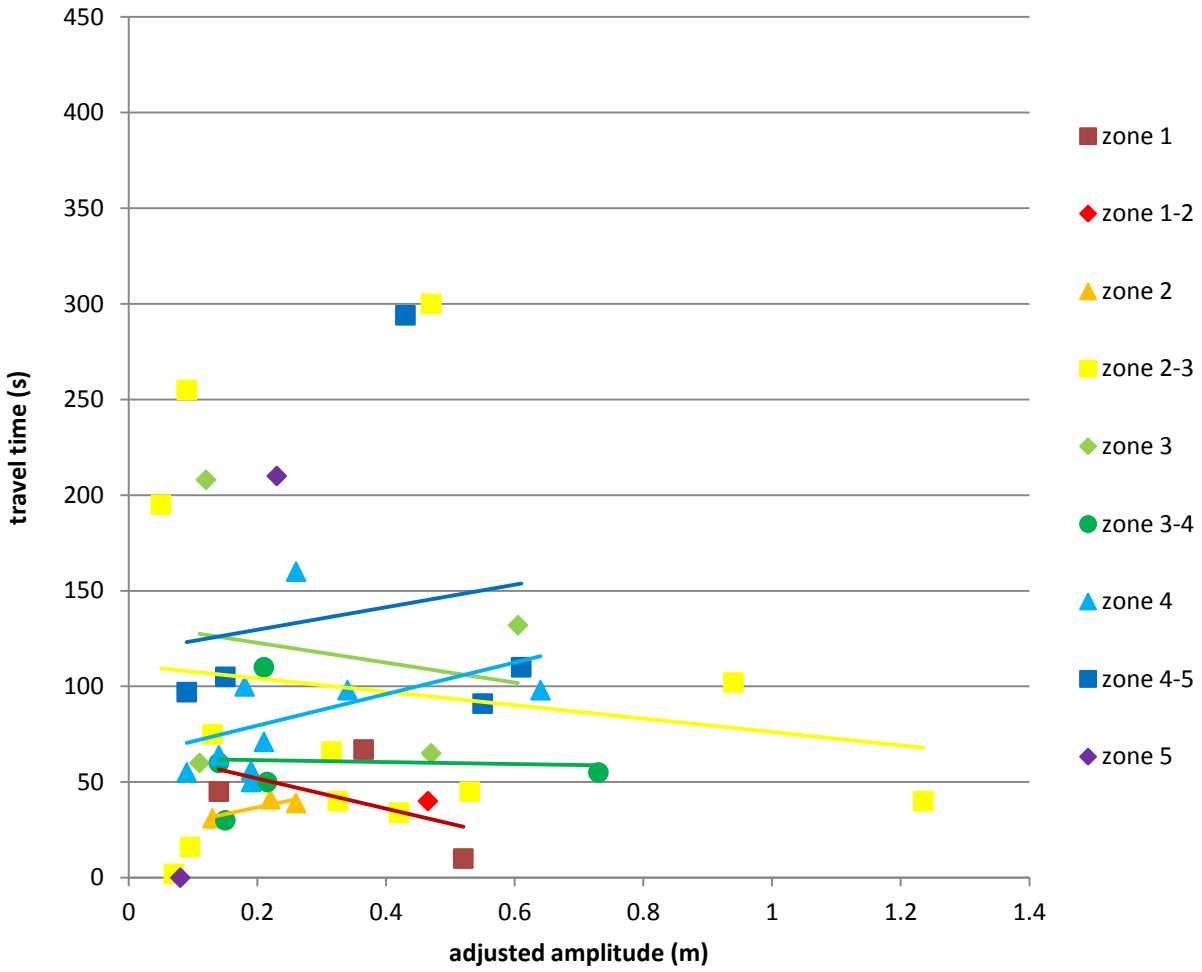

Figure 21. Rock station: Adjusted wave amplitude vs. wave travel time. Data points are exclusively events both visually observed and electronically recorded (paired events). Linear regression equations modeling this relationship are shown in Table 12.

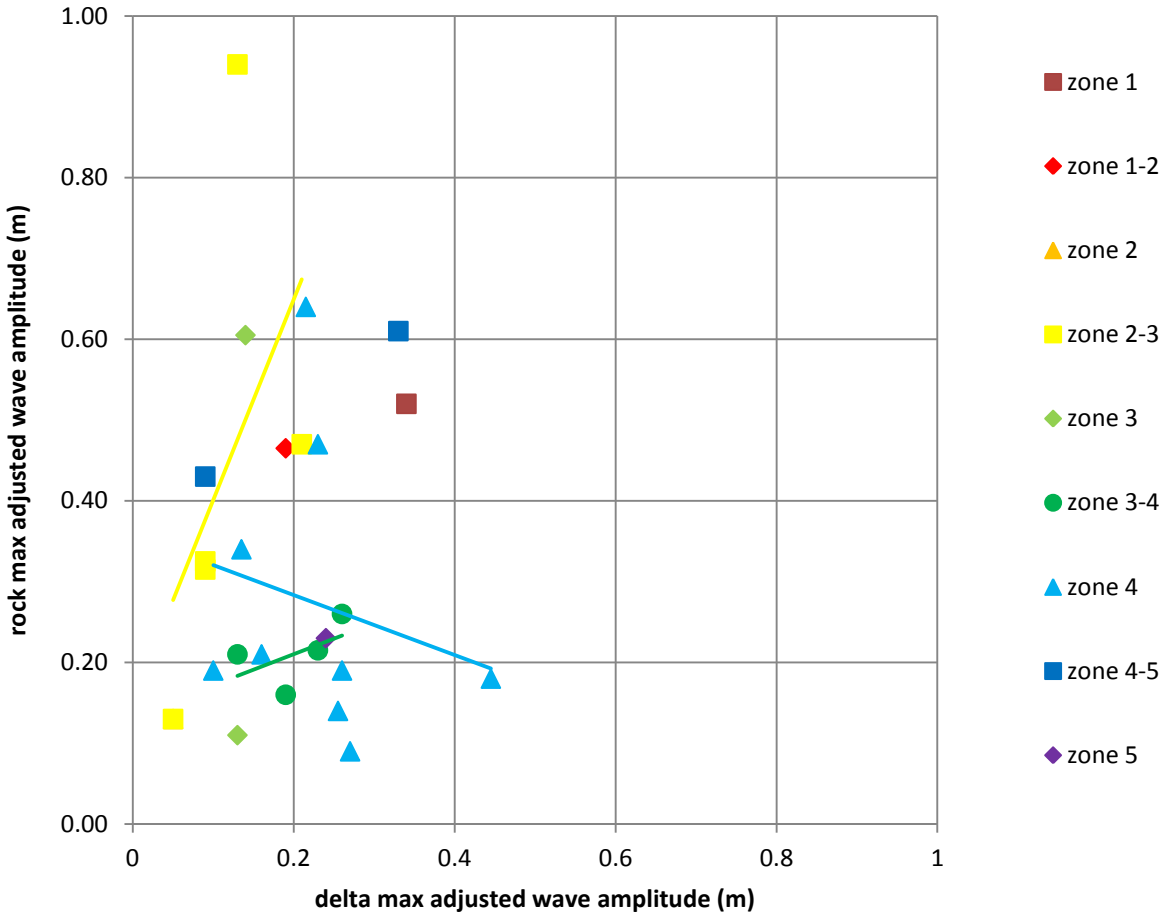

Figure 22. Maximum adjusted wave amplitudes received at Delta vs. rock stations for paired events. Chart indicates that waves originating in the center of the ice front (adjacent to Zone 3) have higher amplitudes at both sites, whereas those substantially closer to one station than the other have an inverse correlation. Correlation coefficients for zones with enough data are: zone 2-3: $R^2 = 0.2406$; zone 3-4: $R^2 = 0.2782$; zone 4: $R^2 = 0.0432$.

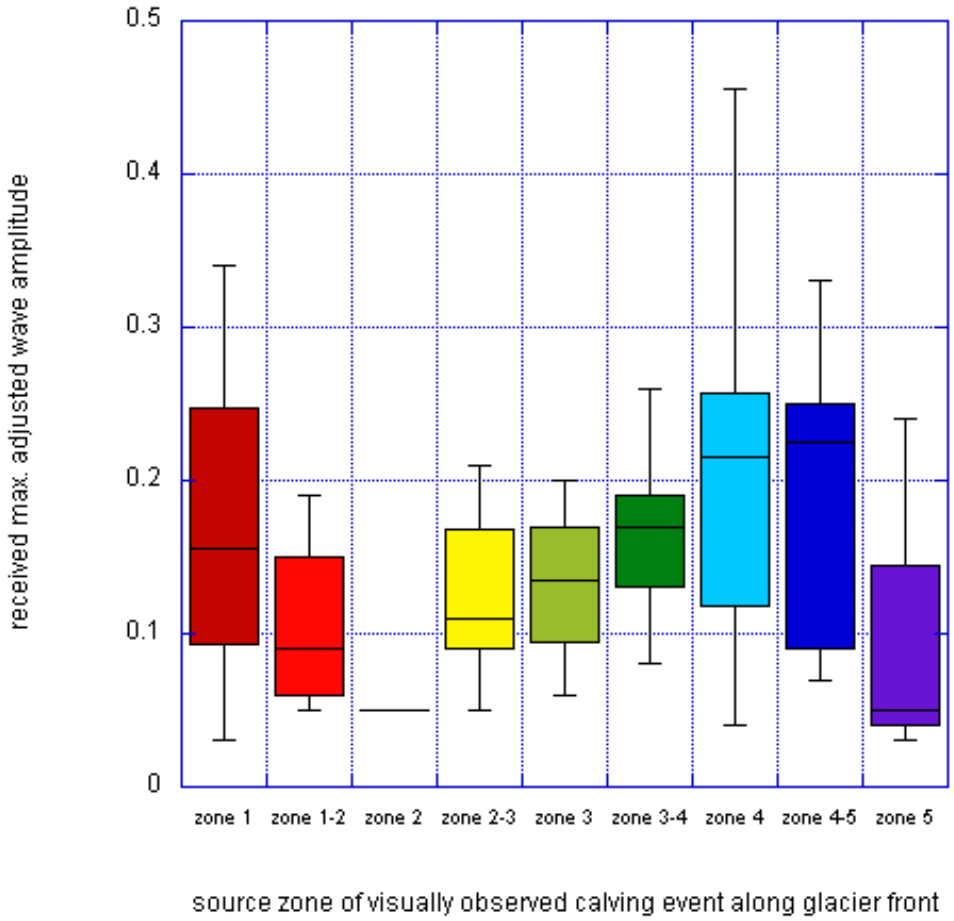

Figure 23. Maximum adjusted wave amplitudes of calving events recorded at the Delta station per source zone of iceberg. Only events that were both visually and electronically recorded (by water depth/pressure loggers) are included. The central black lines in each box represent the mean, the extent of the box represents the distance to one standard deviation, and the bars outside the box represent the extent of the second deviation. Dots outside the box indicate the existence of outliers beyond the second standard deviation.

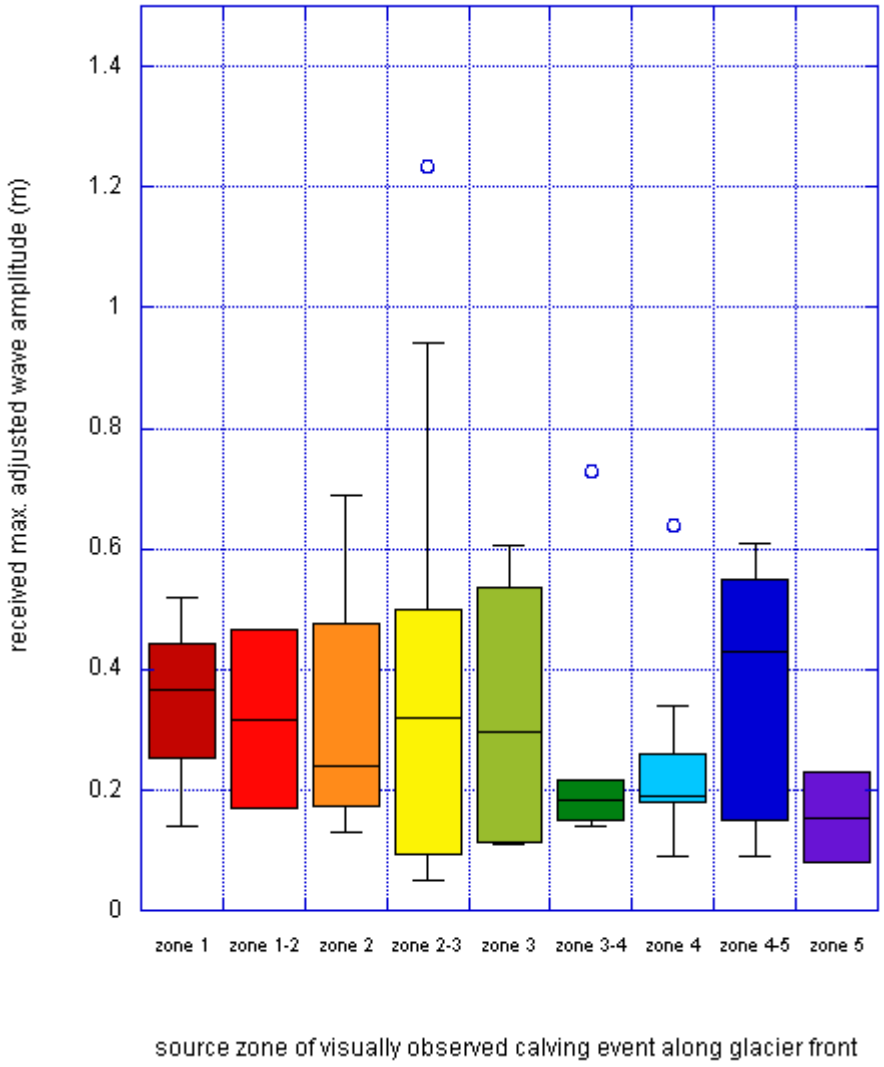

Figure 24. Maximum adjusted wave amplitudes of calving events recorded at the rock station per source zone of iceberg. Only events that were both visually and electronically recorded (by water depth/pressure loggers) are included. The central black lines in each box represent the mean, the extent of the box represents the distance to one standard deviation, and the bars outside the box represent the extent of the second deviation. Dots outside the box indicate the existence of outliers beyond the second standard deviation.

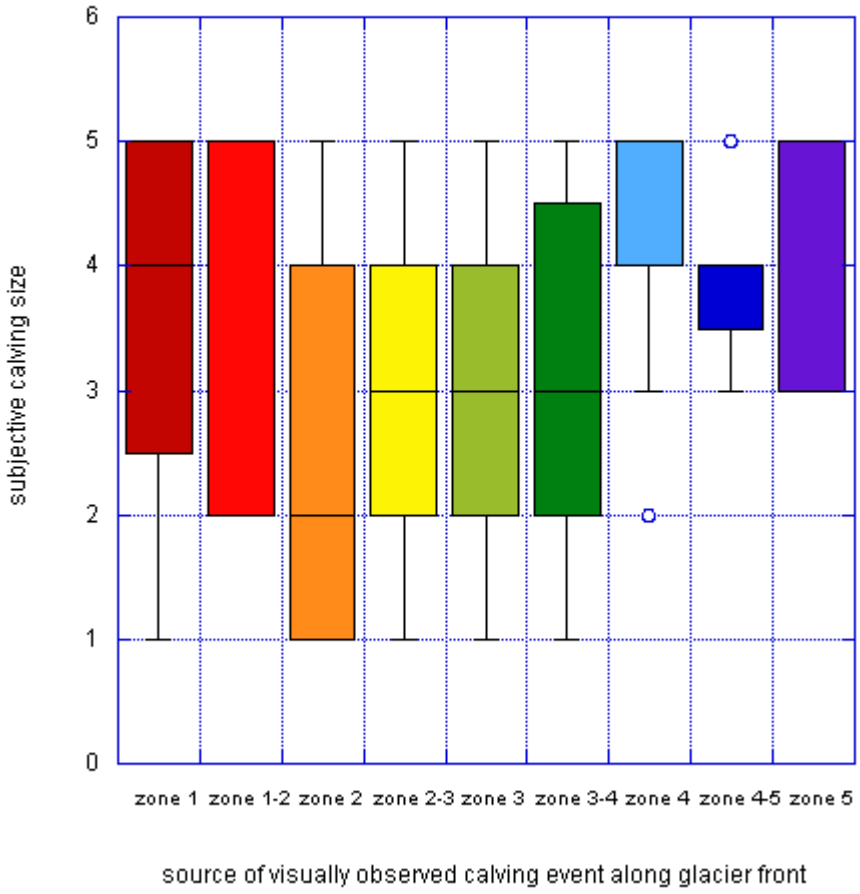

Figure 25. Range of sizes of visually observed calving events by zone of origination. Size used is the subjective size assigned by observation. The central black lines in each box represent the mean, the extent of the box represents the distance to one standard deviation, and the bars outside the box represent the extent of the second deviation. Dots outside the box indicate the existence of outliers beyond the second standard deviation.

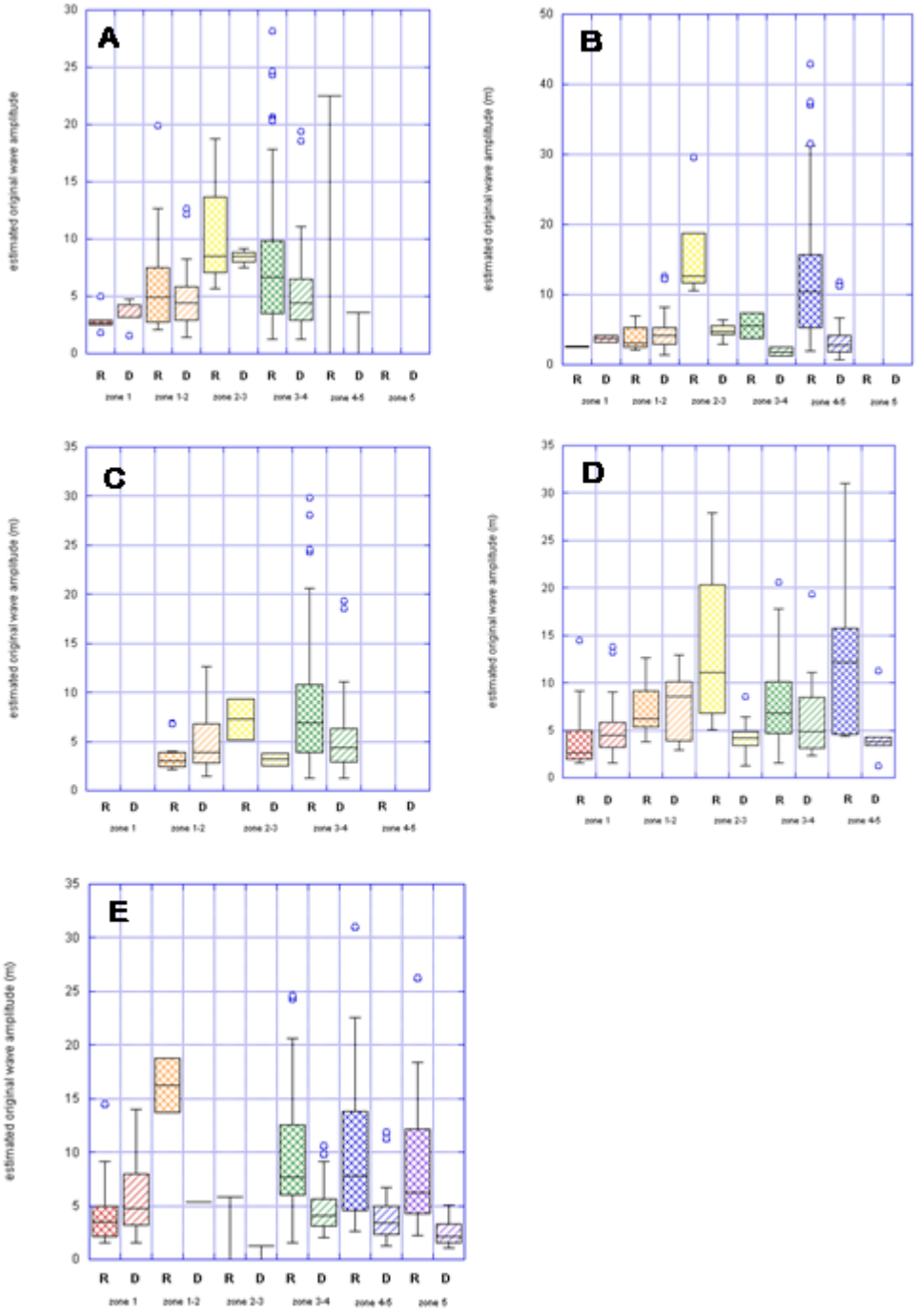

Figure 26. Estimated original wave amplitudes by inversion from received amplitudes, according to each boundary model. Models are Deep Water/Transitional at 50m (A), 30m (B), and 20m (C); Shallow Water (D); and Real Data-zoneadd (E). The central black lines in each box represent the mean, the extent of the box represents the distance to one standard deviation, and the bars outside the box represent the extent of the second deviation. Dots outside the box indicate the existence of outliers beyond the second standard deviation.

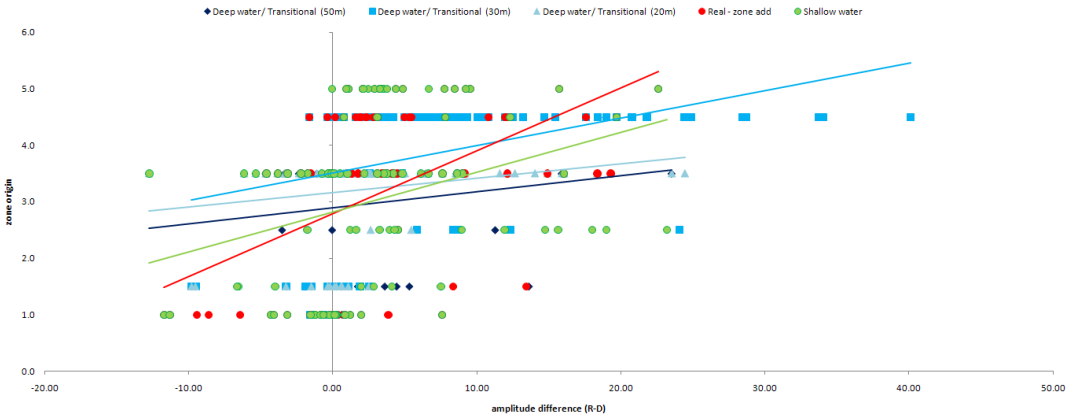

Figure 27. Difference in estimated original wave amplitude by each station compared with the interpreted source of the wave.

TABLES

Table 1. Coordinates of key mooring stations and glacier front zone boundaries. Shown in UTM coordinates, calculated from ASTER image.

	N	E
Rock	446780.8	8759250
Delta	445705.2	8756762
1	447017.7	8759241
1/2	446890.1	8758813
2/3	446744.3	8758257
3/4	446598.5	8758257
4/5	446325	8756944
5	446015.1	8756151

Table 2. Calculated transect distances in meters.

Transects	sqrt=d
R-D	2710.846
R-1	237.1602
R-1/2	450.9758
R-2/3	994.1838
R-3/4	1010.101
R-4/5	2350.653
R-5	3192.22
D-1	2805.236
D-1/2	2368.541
D-2/3	1820.504
D-3/4	1741.386
D-4/5	646.0608
D-5	684.8258

Table 3. Calculated surface wave travel time based on λ=20m. Average depth along the transect is estimated from the bathymetry map in Figure 4. The equation $t = \frac{d}{v}$ (where *d* represents the distance reported in Table 2) was used to calculate the travel time.

Transect	Avg. Depth (m)	velocities (m/s)			travel times (s)		
		Deep water	Transitional	Shallow water	Deep water	Transitional	Shallow water
R-D	60	5.5852	5.5852	24.2487	485.3630	485.3630	111.7934
R-1	20	5.5852	5.5852	14.0000	42.4623	42.4625	16.9400
R-1/2	45	5.5852	5.5852	21.0000	80.7449	80.7449	21.4750
R-2/3	50	5.5852	5.5852	22.1359	178.0035	178.0035	44.9126
R-3/4	45	5.5852	5.5852	21.0000	180.8534	180.8534	48.1001
R-4/5	60	5.5852	5.5852	24.2487	420.8723	420.8723	96.9393
R-5	65	5.5852	5.5852	25.2389	571.5506	571.5506	126.4804
D-1	55	5.5852	5.5852	23.2164	502.2631	502.2631	120.8301
D-1/2	55	5.5852	5.5852	23.2164	424.0751	424.0751	102.0203
D-2/3	50	5.5852	5.5852	22.1359	325.9519	325.9519	82.2420
D-3/4	70	5.5852	5.5852	26.1916	311.7863	311.7863	66.4864
D-4/5	45	5.5852	5.5852	21.0000	115.6739	115.6739	30.7648
D-5	15	5.5852	5.5847	12.1244	122.6146	122.6245	56.4835

Table 4. Calculated and observed wave travel-time differences for various wavelengths. Tables 1 and 2 illustrate the constraints on these models, and the underlying equations for Deep Water, Transitional Deep Water-to-Shallow water are given in Eqs. 3-5. The Real-mean and Real-zoneadd models are derived from the analysis of paired events (events both visually observed and tide gauge-recorded). Differences are Rocktime-Deltatime, so negative values have a shorter travel time to arrive at the Rock station while positive values have a shorter travel time to arrive at the Delta Station, relative to the opposite station in that relationship.

Deep Water:

Wavelength (m) ->	**50m**	**40m**	**30m**	**20m**	**10m**	**real-mean**	**real-zoneadd**
Zone 1	-290.80	-325.12	-375.42	-459.80	-650.25	-80	-75
Zone 1-2	-217.14	-242.77	-280.32	-343.33	-485.54	-70	-63
Zone 2-3	-93.57	-104.61	-120.79	-147.94	-209.23	-98	-57
Zone 3-4	-82.81	-92.58	-106.90	-130.93	-185.17	30	35
Zone 4-5	193.02	215.80	249.19	305.19	431.61	91	51
Zone 5	283.93	317.44	366.55	448.93	634.89	70	86

Transitional deep- to shallow-water:

Wavelength (m) ->	**50m**	**40m**	**30m**	**20m**	**10m**	**real-mean**	**real-zoneadd**
Zone 1	-290.62	-325.07	-375.41	-459.80	-650.25	-80	-75
Zone 1-2	-217.14	-242.77	-280.32	-343.33	-485.54	-70	-63
Zone 2-3	-93.57	-104.61	-120.79	-147.94	-209.23	-98	-57
Zone 3-4	-82.80	-92.58	-106.90	-130.92	-185.16	30	35
Zone 4-5	193.02	215.80	249.19	305.19	431.61	91	51
Zone 5	282.12	316.66	366.36	448.92	634.89	70	86

Shallow water:

Wavelength (m) ->	**50**	**40**	**30**	**20**	**10**	**real-mean**	**real-zoneadd**
Zone 1	-103.89	-103.89	-103.89	-103.89	-103.89	-80	-75
Zone 1-2	-80.54	-80.54	-80.54	-80.54	-80.54	-70	-63
Zone 2-3	-37.32	-37.32	-37.32	-37.32	-37.32	-98	-57
Zone 3-4	-18.38	-18.34	-18.38	-18.38	-18.38	30	35
Zone 4-5	66.17	66.17	66.174	66.17	66.17	91	51
Zone 5	69.99	69.99	69.99	69.99	69.99	70	86

Table 5. Table of correlation coefficients between environmental variables and calving rates. Above the diagonal black divider in the lighter gray region, **r** is reported; below the black bar, $\mathbf{R^2}$ is reported for each pairing. Numbers are colored in grayscale in relation to their relative statistical significance of the correlation. The time series representation of each factor is included in this paper. Delta and Rock calving rates are quarter-daily (6-hour periods) to match the precipitation and temperature data resolution. Underlined values are relationships between environmental variables and calving measurements that are greater than r=|0.10|

		Precipitation time (minutes)	Air temperature (ºC)	Tidal height (m)	Delta Station				Rock Station				Delta calving rate	Rock calving rate
					Sum	Avg.	Max.	Count	Sum	Avg.	Max.	Count		
Precipitation time (minutes)		1.00	-0.17	0.04	0.13	-0.07	-0.05	0.20	-0.15	-0.03	-0.20	-0.11	0.23	0.06
Air temperature (ºC)			1.00	-0.01	-0.14	0.20	0.05	-0.28	0.31	0.17	0.26	0.24	-0.27	0.13
Tidal height (m)				1.00	0.07	0.21	0.05	-0.10	-0.02	0.03	0.07	-0.04	-0.09	-0.13
Delta Station	Sum				1.00	0.61	0.77	0.82	0.49	0.43	0.35	0.38	0.73	0.39
	Avg				0.38	1.00	0.71	0.11	0.54	0.41	0.45	0.46	0.12	0.41
	Max				0.59	0.51	1.00	0.46	0.53	0.30	0.42	0.45	0.39	0.47
	Count				0.67		0.21	1.00	0.25	0.21	0.11	0.19	0.87	0.22
Rock Station	Sum				0.24	0.29	0.28		1.00	0.51	0.78	0.87	0.18	0.74
	Avg				0.18	0.17			0.26	1.00	0.60	0.13	0.20	0.14
	Max				0.12	0.20	0.18		0.61	0.36	1.00	0.61	0.08	0.53
	Count				0.14	0.21	0.20		0.77		0.37	1.00	0.10	0.90
Delta calving rate					0.54		0.15	0.76					1.00	0.24
Rock calving rate					0.15	0.17	0.22		0.54		0.28	0.82		1.00

Table 6. Correlations (**r**) between maximum daily tide and daily calving measures at Rock and Delta stations at various lag intervals. Underlined numbers indicate weak (>0.2) correlations, bolded numbers indicate moderate (>0.4) correlations, and bold-italicized numbers indicate strong (>0.7) correlations.

	daily rate		sum		average		max	
lag	**delta**	**Rock**	**delta**	**Rock**	**delta**	**Rock**	**delta**	**Rock**
none	0.059	0.336	0.224	0.149	0.195	**0.413**	0.050	0.078
1 day	**0.514**	**0.468**	**0.442**	0.235	0.032	**0.352**	0.232	0.260
2 days	**0.584**	**0.517**	0.327	0.274	0.303	**0.392**	0.242	0.247
3 days	**0.521**	**0.465**	0.208	**0.433**	**0.403**	**0.433**	0.250	0.078
4 days	0.290	0.246	0.082	0.241	0.275	***0.686***	0.250	0.171
5 days	0.088	0.203	0.209	**0.407**	0.050	***0.679***	0.281	0.098
6 days	**0.558**	0.122	***0.700***	0.208	0.121	0.293	0.185	0.001
7 days	***0.719***	0.177	***0.849***	0.293	0.143	0.155	**0.410**	0.153

Table 8. ANOVA Single Factor: Calving rate at Rock station during different tidal phases

Groups	*Count*	*Sum*	*Average*	*Variance*		
High tide	13	159	12.230	57.192		
Falling tide	13	204	15.692	26.897		
Low tide	13	222	17.077	55.410		
Rising tide	13	209	16.077	30.910		
Source of Variation	*SS*	*df*	*MS*	*F*	*P-value*	*F crit*
Between Groups	173.307	3	57.769	1.356	0.267	2.798
Within Groups	2044.92	48	42.603			
Total	2218.23	51				

Table 9. ANOVA Single Factor: Calving event amplitude at Delta station during different tidal phases.

Groups	*Count*	*Sum*	*Average*	*Variance*
High tide	14	1.520	0.108	0.001
Falling tide	14	1.532	0.109	0.001
Low tide	14	1.580	0.112	0.000
Rising tide	14	1.403	0.100	0.001

ANOVA

Source of Variation	*SS*	*df*	*MS*	*F*	*P-value*	*F crit*
Between Groups	0.001	3	0.000	0.441	0.725	2.783
Within Groups	0.0477	52	0.001			
Total	0.0489	55				

Table 10. ANOVA Single Factor: Calving event amplitude at Rock station during different tidal phases.

Groups	*Count*	*Sum*	*Average*	*Variance*
High tide	13	2.563	0.197	0.009
Falling tide	13	2.692	0.207	0.004
Low tide	13	2.495	0.192	0.001
Rising tide	13	2.487	0.191	0.007

Source of Variation	*SS*	*df*	*MS*	*F*	*P-value*	*F crit*
Between Groups	0.002	3	0.001	0.134	0.939	2.798
Within Groups	0.247	48	0.005			
Total	0.249	51				

Table 11. Wave travel time equations per zone to delta station for events observed visually and electronically recorded

Zone	Equation	R^2	# events recorded
1	y = -84.69x + 90.15	0.0436	3
1-2	y = -36.52x + 114.83	0.0200	4
2	insufficient data	insufficient data	4
2-3	y = 672.71x + 96.81	0.1304	7
3	y = 154.18x + 39.32	0.4578	4
3-4	y = -281.55x + 103.06	0.3854	9
4	y = -7.47x + 50.801	0.0011	15
4-5	y = -362.59x + 139.78	0.4905	5
5	insufficient data	insufficient data	2

Table 12. Wave travel time equations per zone to Rock station for events observed visually and electronically recorded

Zone	Equation	R^2	# events recorded
1	y = -78.45x + 67.47	0.2719	3
1-2	insufficient data	insufficient data	2
2	y = 69.93x + 22.78	0.7742	4
2-3	y = -34.97x + 111.11	0.0175	12
3	y = -51.88x + 133.18	0.0349	4
3-4	y = -16.67x + 70.29	0.0172	6
4	y = 82.36x + 63.05	0.147	9
4-5	y = 58.77x + 117.89	0.0253	5
5	insufficient data	insufficient data	2

Table 13. Comparisons of the proportions of localizations inverted to each zone, depending upon the boundary conditions used. The boundary limits for each model [equations 3-5] are shown in Table 6. The proportions for visually observed events are included for comparison, and the grey shaded boxes represent the modeled proportion closest to the visually observed proportions. The visually observed proportions for the higher-resolution boundaries are shown in Table 14.

	Deep water/ Transitional (50m)		Deep water/ Transitional (30m)		Deep water/ Transitional (20m)		Shallow water		Real - zone add		Visually observed	
zone	**#**	**%**	**#**	**%**	**#**	**%**	**#**	**%**	**#**	**%**	**#**	**%**
1	5	5.10	2	2.04	0	0.00	22	22.45	29	29.59	8	8.60
1-2	19	19.39	14	14.29	12	12.24	7	7.14	2	2.04	16	17.20
2-3	3	3.06	5	5.10	2	2.04	14	14.29	1	1.02	17	18.28
3-4	70	71.43	2	2.04	84	85.71	28	28.57	28	28.57	22	23.66
4-5	1	1.02	75	76.53	0	0.00	5	5.10	22	22.45	25	26.88
5	0	0.00	0	0.00	0	0.00	22	22.45	16	16.33	5	5.38
Total	98	100.0	98	100.0	98	100.0	98	100.0	98	100.0	93	100.0

Table 14. Proportion of visually observed calving events, reported by zone of origination. These are not limited to those confirmed by tide gauge recordings.

	Visually observed	
	#	**%**
zone 1	8	8.60
zone 1-2	6	6.45
zone 2	10	10.75
zone 2-3	17	18.28
zone 3	6	6.45
zone 3-4	16	17.20
zone 4	18	19.35
zone 4-5	7	7.53
zone 5	5	5.38
Total	93	100.00

Table 15. Multiple-Regression Model: Dependent Variable is Quarter-daily Delta station calving rate				
R^2 = 0.1230; R^2 (adjusted) = 0.0761				
Source	**Sum of Squares**	**df**	**Mean Square**	**F-ratio**
Regression	113.5690	3.0000	37.8563	2.6191 (Sig=0.0597)
Residual	809.4144	56.0000	14.4538	
Variable	**Coefficient**	**s.e. of Coefficient**	**t-ratio**	**P-value**
Intercept	14.2391	2.5213	5.6475	0.0000
Precipitation time (minutes)	0.0274	0.0176	1.5524	0.1262
Air temperature (ºC)	-0.6428	0.3359	-1.9133	0.0608
Tidal height (m)	-1.7175	2.0232	-0.8489	0.3995

Table 16. Multiple-Regression Model: Dependent Variable is Quarter-daily Rock station calving rate				
R^2 = 0.0388; R^2 (adjusted) = -0.0166				
Source	**Sum of Squares**	**df**	**Mean Square**	**F-ratio**
Regression	95.2683	3.0000	31.7561	0.7001 (Sig=0.5562)
Residual	2358.5710	52.0000	45.3571	
Variable	**Coefficient**	**s.e. of Coefficient**	**t-ratio**	**P-value**
Intercept	11.1769	5.8837	1.8996	0.0630
Precipitation time (minutes)	-0.0212	0.0322	-0.6581	0.5134
Air temperature (ºC)	0.9335	0.9037	1.0330	0.3064
Tidal height (m)	-1.5791	3.6205	-0.4362	0.6645

REFERENCES CITED

Alley, R. B., et al., 2008, A Simple Law for Ice-Shelf Calving: Science, vol. 322, p. 1344.

Amundson, A.M., et al., 2008, Glacier, fjord, and seismic response to recent large calving events, Jakobshavn Isbrae, Greenland: Geophysical Research Letters, vol. 35, L22501, doi: 10.1029/2008GL035281.

Aniya, M., et al., 2007, Glaciological and geomorphological studies at Glaciar Exploradores, Hielo Patagónico Norte, and Glaciar Perito Moreno, Hielo Patagónico Sur, South America, during 2003-2005: Bulletin of Glaciological Research , vol. 24: p. 95-107.

Bamber, J. L., et al., 2007, Rapid response of modern day ice sheets to external forcing: Earth and Planetary Science Letters, vol. 257, p. 1–13.

Benn, D.I., et al., 2007, 'Calving laws', 'sliding laws' and the stability of tidewater glaciers: Annals of Glaciology, vol. 34, p. 123-130.

Benn, D.I., et al., 2007, Calving processes and the dynamics of calving glaciers: Earth-Science Reviews, vol. 82, p. 143–179.

Blaszczyk, M., et al., 2009, Tidewater glaciers of Svalbard: Recent changes and estimates of calving fluxes: Polish Polar Science, vol. 30, no. 2, pp. 85–142.

Brown, C.S., et al., 1982, Calving speed of Alaska Tidewater Glaciers, with Application to Columbia Glacier: Studies of Columbia Glacier, Geological Survey Professional Paper 1258-C, 20 p.

Dowdeswell, J.A., et al., 1997, The Mass Balance of Circum-Arctic Glaciers and Recent Climate Change: Quaternary Research, vol. 48, p. 1-14.

Dowdeswell, J.A., Forsberg, C., 1992, The size and frequency of icebergs and bergy bits derived from tidewater glaciers in Kongsfjorden, northwest Spitsbergen: Polar Research, vol. 11, no. 2, 81-91.

Frezotti, M., 1997, Ice front fluctuation, iceberg calving flux, and mass balance of Victoria Land glaciers: Antarctic Science, vol. 9, no. 1, p. 61-73.

Glasser, N.F., Hambrey, M.J., 2001, Tidewater glacier beds: insights from iceberg debris in Kongsfjorden, Svalbard: Journal of Glaciology, vol. 147, no. 157, p. 295-301.

Hagen, J.O., et al., 1999, Mass Balance Methods on Kongsvegen, Svalbard: Geografiska Annaler. Series A, Physical Geography, vol. 81, no. 4, p. 593-601.

Hagen, J.O., et al., 2003, On the Net Mass Balance of the Glaciers and Ice Caps in Svalbard, Norwegian Arctic: Arctic, Antarctic, and Alpine Research, vol. 35, no. 2, p. 264–270.

Hagen, J.O., et al., 2005, Geometry changes on Svalbard glaciers: mass-balance or dynamic response?: Annals of Glaciology, vol. 42, p. 255-261.

Haresign, E., Warren, C.R., 2005, Melt rates at calving termini: a study at Glaciar Leon, Chilean Patagonia *in* Harris, C., Murton, J.B., (eds.), 2005, Cryospheric Systems: Glaciers and Permafrost: Geological Society, London, Special Publications, vol. 242, p. 99-109.

Howat, I.M., Joughin, I., and Scambos, T.A., 2007, Rapid Changes in Ice Discharge from Greenland Outlet Glaciers: Science, v. 315, p. 1559-1561.

Howat, I.M., Joughin, I., Fahnestock, M., Smith, B.E., and Scambos, T.A., 2008, Synchronous retreat and acceleration of southeast Greenland outlet glaciers 2000–06: ice dynamics and coupling to climate: Journal of Glaciology, v. 54, no. 187, p. 646-660.

Ilzuka, Y., Kobayashi, S., and Naruse, R., 2004, Water surface waves induced by calving events at Perito Moreno Glacier, southern Patagonia: Bulletin of Glaciological Research, v. 21, p. 91-96.

Joughin, I., Das, S.B., King, M.A., Smith, B.E., Howat, I.M., Moon, T., 2008, Seasonal Speedup Along the Western Flank of the Greenland Ice Sheet: Science, v. 320, p. 781-783.

Kehrl, L.M., 2010, Fjord floor landforms and processes at the termini of Kongsvegen and Kronebreen Glaciers, Svalbard [Presented Abstract]: Arctic Workshop 2010.

Krimmel, R.M., Vaughn, B.H., 1987, Columbia Glacier, Alaska; changes in velocity 1977–1986: Journal of Geophysical Research, v. 92, no. B9, p. 8961–8968.

LeFauconnier, B., Hagen, J.O., and Rudant, J.P., 1994, Flow speed and calving rate of Kongsbreen glacier, Svalbard, using SPOT images: Polar Research, p. 59-65.

Legresy, B., Wendt, A., Tabacco, I., Remy, F., and Dietrich, R., 2004, Influence of tides and tidal current on Mertz Glacier, Antarctica: Journal of Glaciology, v. 50, no. 170, p. 427-435.

Marshburn, H.L., 2010, Glaciomarine Oceanographic and Suspended Sediment Dynamics, Kongsbreen system, Svalbard [Presented Abstract]: Arctic Workshop 2010.

Meier, M.F., and Post, A., 1987, Fast Tidewater Glaciers: Journal of Geophysical Research, v. 92, no. B9, p. 9051-9058.

Meier, M.F., Dyurgerov, M.B., Rick, U.K., O'Neel, S., Pfeffer, W.T., Anderson, R.S., Anderson, S.P., and Glazovsky, A.F., 2007, Glaciers Dominate Eustatic Sea-Level Rise in the 21st Century: Science, v. 317, no. 5841, p. 1064-1067.

Nick, F.M., and Oerlemans, J., 2006, Dynamics of tidewater glaciers: comparison of three models: Journal of Glaciology, v. 52, no. 177, p. 183-190.

Nilsen, F., Cottier, F., Skogseth, R., and Mattsson, S., 2008, Fjord-shelf exchanges controlled by ice and brine production: The interannual variation of Atlantic Water in Isfjorden, Svalbard: Continental Shelf Research, v. 28, p. 1838-1853.

O'Neel, S., Echelmeyer, K.A., Motyka, R.J., 2001. Short-term flow dynamics of a retreating tidewater glacier: LeConte Glacier, Alaska, U.S.A. Journal of Glaciology 47, 567–578.

O'Neel, Shad, et al., 2003, Short-term variations in the calving of a tidewater glacier: LeConte Glacier, Alaska, U.S.A.: Journal of Glaciology, v. 49, no. 167, p. 587-598.

Pralong, A., and Funk, M., 2005, Dynamic damage model of crevasse opening and application to glacier calving: Journal of Geophysical Research, v. 110, B01309, 12 p.

Qamar, A., 1988, Calving icebergs: A source of low-frequency seismic signals from Columbia Glacier, Alaska: Journal of Geophysical Research, v. 93, no. B6, p. 6615-6623.

Rolstad, C., and Norland, R., 2009, Ground-based interferometric radar for velocity and calving-rate measurements of the tidewater glacier at Kronebreen, Svalbard: Annals of Glaciology, v. 50, p. 47-54.

Skvarca, P., and Naruse, R., 1997, Dynamic behavior of Glaciar Perito Moreno, southern Patagonia: Annals of Glaciology, v. 24, p. 268-271.

Sund, M., and Eiken, T., 2010, Recent surges on Blomstrandbreen, Comfortlessbreen, and Nathorstbreen, Svalbard: Journal of Glaciology, v. 56, no. 195, p. 182-184.

Sund, M., Eiken, T., Hagen, J.O., and Kaab, A., 2009, Svalbard surge dynamics derived from geometric changes: Annals of Glaciology, v. 50, no. 52, p. 50-60.

Thomas, R.H., 2007, Tide-induced perturbations of glacier velocities: Global and Planetary Change, v. 57, p. 217-224.

Trusel, L.D., R.D. Powell, R.M. Cumpston, and J. Brigham-Grette, 2010, in press, Modern glacimarine processes and potential future behaviour of Kronebreen and Kongsvegen Polythermal Tidewater Glaciers, Kongsfjorden, Svalbard: Geol. Soc. London.

Van der Veen, C.J., 2002, Calving glaciers: Progress in Physical Geography, v. 26, no. 1, p. 96-122.

Warren, C.R., N. F. Glasser, S. Harrison,V.Winchester, A.R. Kerr, and Rivera, A., 1995, Characteristics of tide-water calving at Glaciar San Rafael, Chile: Journal of Glaciology, v. 41, no. 138, p. 273-289.

Warren, C.R., Aniya, M., 1999, The calving glaciers of southern South America: Global and Planetary Change, v. 22, p. 57-77.

Weiss, J., 2004, Subcritical crack propagation as a mechanism of crevasse formation and iceberg calving: Journal of Glaciology, v. 50, p. 109-115.